12

VSC-TR-82-20

A MODEL FOR TECTONIC STRAIN RELEASE FROM EXPLOSIONS IN COMPLEX PRESTRESS FIELDS APPLIED TO ANOMALOUS SEISMIC WAVES FROM NTS AND EASTERN KAZAKH EXPLOSIONS

J. L. Stevens

TECHNICAL REPORT

SYSTEMS, SCIENCE AND SOFTWARE
P. O. Box 1620
La Jolla, California 92038

January 1982

Approved for Public Release,
Distribution Unlimited

Monitored by:

VELA Seismological Center
312 Montgomery Street
Alexandria, Virginia 22314

Unclassified

SECURITY CLASSIFICATION OF THIS PAGE (When Data Entered)

REPORT DOCUMENTATION PAGE	READ INSTRUCTIONS BEFORE COMPLETING FORM
1 REPORT NUMBER: VSC-TR-82-20	2 GOVT ACCESSION NO: AD-A118503
3 RECIPIENT'S CATALOG NUMBER:	
4. TITLE (and Subtitle): A Model for Tectonic Strain Release from Explosions in Complex Prestress Fields Applied to Anomalous Seismic Waves from NTS and Eastern Kazakh Explosions	5 TYPE OF REPORT & PERIOD COVERED: Technical Report
	6. PERFORMING ORG. REPORT NUMBER: SSS-R-82-5358
7 AUTHOR(s): J. L. Stevens	8. CONTRACT OR GRANT NUMBER(s): F08606-79-C-0008
9 PERFORMING ORGANIZATION NAME AND ADDRESS: Systems, Science and Software, P.O. Box 1620, La Jolla, California 92038	10 PROGRAM ELEMENT, PROJECT, TASK AREA & WORK UNIT NUMBERS: ARPA Order No. 2551, Program Code No. 6H189
11 CONTROLLING OFFICE NAME AND ADDRESS: VELA Seismological Center, 312 Montgomery Street, Alexandria, Virginia 22314	12. REPORT DATE: January 1982
	13. NUMBER OF PAGES: 75
14. MONITORING AGENCY NAME & ADDRESS(if different from Controlling Office)	15 SECURITY CLASS. (of this report): Unclassified
	15a. DECLASSIFICATION/DOWNGRADING SCHEDULE

16 DISTRIBUTION STATEMENT (of this Report)

Approved for Public Release, Distribution Unlimited.

17 DISTRIBUTION STATEMENT (of the abstract entered in Block 20, if different from Report)

18. SUPPLEMENTARY NOTES

19 KEY WORDS (Continue on reverse side if necessary and identify by block number)

Prestress
Tectonic strain release
Underground nuclear explosions
Explosion seismology

20. ABSTRACT (Continue on reverse side if necessary and identify by block number)

Anomalous surface waves including Love waves and phase reversed Rayleigh waves have been observed from explosions at NTS and from the eastern Kazakh areas of the Soviet Union. In this report we use a linear model for tectonic strain release to estimate the amount and type of prestress required to produce these anomalies. An important use of these results is to guide the input to fully nonlinear simulations of an explosion detonated in a prestressed environment.

(Continued)

DD FORM 1 JAN 73 1473 EDITION OF 1 NOV 65 IS OBSOLETE

Unclassified

SECURITY CLASSIFICATION OF THIS PAGE (When Data Entered)

ABSTRACT: (Continued)

Tectonic strain release adds energy to the explosion component of the seismic radiation because elastic energy stored in the medium is released when a zone of weakened material strength is created by the explosion. In the model, this zone is treated as if it were a spherical cavity with the dimensions of the explosion-produced failure zone. This effective cavity radius requires independent constraints which can be provided by nonlinear simulations.

General conclusions are as follows:

In the presence of stress concentrations, tectonic release enhances high frequency radiation in preferred directions.

Compressive stress concentrations reduce body wave amplitudes while tensile stress concentrations amplify body waves.

Long period tectonic surface waves depend only on the average prestress field and are unaffected by stress heterogeneity.

The tectonic surface waves reduce to a monopole plus a quadrupole field superimposed on the explosion monopole.

Specific conclusions are as follows:

Rayleigh wave reversals or factor of two enhancements (depending on the horizontal prestress being compressive or tensile relative to the hydrostatic prestress) can be obtained with homogeneous or average shear stresses of about 50 bars assuming that the effective cavity radius is equal to the explosion elastic radius.

A maximum local shear stress of about a kilobar is required before the tectonic component of body waves becomes comparable in size to the explosion body waves. The average prestress may be much lower, however.

The anomalous body wave, Love wave and Rayleigh wave radiation from PILEDRIVER can be simultaneously explained by a compressive stress concentration of about a kilobar to the northeast of the explosion.

AFTAC Project Authorization No. VT/0712/B/PMP
ARPA Order No. 2551, Program Code No. 6H189
Effective Date of Contract: November 17, 1978
Contract Expiration Date: November 15, 1981
Amount of Contract: $1,816,437
Contract No. F08606-79-C-0008
Principal Investigator and Phone No.
Dr. J. Theodore Cherry, (714) 453-0060
Project Scientist and Phone No.
Mr. Brian W. Barker, (202) 325-7581

This research was supported by the Advanced Research Projects Agency of the Department of Defense and was monitored by AFTAC/VSC, Patrick Air Force Base, Florida 32925, under Contract No. F08606-79-C-0008.

W/O 11098

TABLE OF CONTENTS

LIST OF ILLUSTRATIONS

LIST OF TABLES

I. INTRODUCTION

Rygg (1979) reports the observation of two phase reversed Rayleigh waves from underground nuclear explosions in the eastern Kazakh area of the Soviet Union. Patton (1980) reports that several additional explosions from the same area also appear to have Rayleigh wave reversals. Figure 1.1 shows two Rayleigh waves from eastern Kazakn (Shagan River) explosions with clearly reversed polarities recorded at Kabul, Afghanistan. Goforth, Rafipour and Herrin (1982), using a phase-matched filter analysis, find phase reversals and time delays of about three seconds for several Shagan River explosions. Such observations have been reported in other areas as well. Perhaps the best documented case of a Rayleigh wave reversal is from the NTS explosion PILEDRIVER (Toksöz and Kehrer, 1972). Rayleigh wave reversals are usually accompanied by the generation of large amplitude Love waves. In the case of PILEDRIVER, a body wave anomaly also occurred, with a strong reduction in amplitude to the Northeast (Hadley and Hart, 1979). Since body wave magnitudes are used to estimate explosion yields, it is very important to understand what variations in body wave amplitudes may accompany surface wave anomalies.

In this report we use a model for tectonic release which can produce Rayleigh wave reversals and large Love waves. The model assumes that when an underground explosion is detonated, a shatter zone (region of weakened material) is formed around the cavity. If the material near the explosion is initially in a strained state, then elastic energy stored in the medium is released in the form of seismic waves. These tectonic surface and body waves interfere with the surface and body waves of the explosion, and will cause Rayleigh wave reversals if the tectonic Rayleigh wave is reversed in polarity and exceeds the explosion Rayleigh wave in amplitude. If the horizontal prestress is compressive compared to the hydrostatic prestress, then the tectonic Rayleigh waves will be reversed in phase compared to the monopole explosion Rayleigh waves. Conversely, a horizontal prestress that is tensile compared to the hydrostatic prestress causes Rayleigh wave amplification.

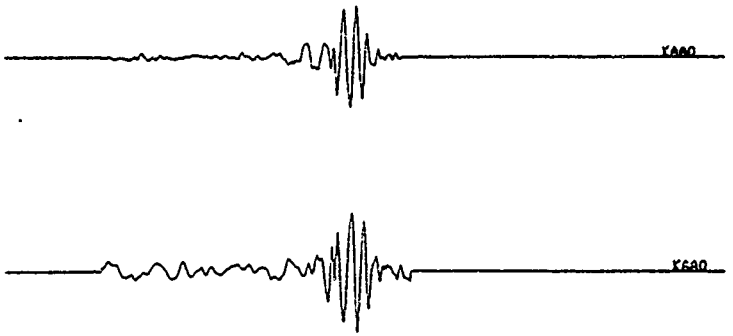

Figure 1.1 Rayleigh waves from two explosions in the eastern Kazakh (Shagan River) area of the Soviet Union which exhibit phase reversals. The two events were recorded at station KAAO on 18 August 1979 and 28 October 1979, respectively.

The explosions which show the greatest amount of tectonic release are those in granite (Toksöz and Kehrer, 1972). For our explosion models, we therefore use two spherically symmetric granite source models — the empirical model of Mueller and Murphy (1971) and a numerical model for partially saturated granite (Bache, Barker, Rimer and Cherry, 1980). We add the wavefield generated by the tectonic release model to these monopole explosion sources in order to determine the effect of model parameters on body waves and surface waves.

The model used here to simulate tectonic release is the sudden creation of a spherical cavity in a prestressed medium (Stevens, 1980). This provides a linear approximation to the complex nonlinear processes which accompany an explosion in a prestressed medium. In this report we use the linear model to estimate the prestress level necessary to cause Rayleigh wave reversals. This estimate may be used to provide a reference level for fully nonlinear simulations of an explosion in a prestressed environment. Nonlinear calculations in turn may be used to provide an estimate of the effective "cavity" radius which is a poorly constrained parameter in the linear model.

Day, Rimer, Cherry and Stevens (1981) performed a two-dimensional nonlinear finite difference calculation of an explosion in a prestressed medium where the prestress consisted of overburden pressure superimposed on a 75 bar shear stress. The results of the calculation show that the effective cavity radius (determined by comparing surface wave amplitudes from the nonlinear simulation with surface wave amplitudes from the linear model used in this report) is about 60 - 80 percent of the elastic radius. Also, the waveforms of long period surface waves found in the nonlinear simulation are almost identical to the waveforms generated using the linear model.

In addition to finding the prestress necessary to cause Rayleigh wave reversals, we also estimate the amplitudes of the associated Love waves and the variations in body wave amplitudes which accompany the reversals. We explicitly include the effects of

nearby stress concentrations and look at the effects of the stress inhomogeneity on body and surface waves.

An important prediction of the work is that an inhomogeneous prestress field should have a much stronger effect on the high frequencies than a homogeneous stress field would have. The body waves can therefore be strongly affected by inhomogeneous stress fields, especially in larger explosions. Also, the variation in body waves can be highly directional with a strong decrease (or increase) of body waves in preferred directions. If a stress concentration is located close to the explosion, the body waves will be most strongly affected in the direction of the stress concentration.

Uniform prestress fields in general should have a much stronger influence on explosion surface waves than on the body waves. Assuming that the region with minimal shear strength extends to the elastic radius, Rayleigh wave reversal may be obtained with a tectonic prestress of about 50 bars. In the linear model, assuming that shatter zone formation is instantaneous, there is no time delay associated with the reversal. A time delay would exist if the shatter zone formed over an extended period of time (e.g., Stevens, 1982).

Because of the boundary condition of vanishing normal and shear tractions at the free surface, the only truly uniform prestress fields which can exist are linear combinations of "strike slip" and uniaxial prestress fields. The tectonic radiation from explosions in these prestress configurations has negligible influence on steeply descending body waves from the explosion. If the prestress field is not quite homogeneous, then the prestress orientation may be different at the explosion depth than at the free surface. Some other prestress orientations can have stronger effects on the explosion body waves. The results of the calculations for all uniform stress fields are summarized in Table 3.3 and Figures 3.4 through 3.7.

Nonuniform prestress fields can occur in many different ways. They always require some sort of dislocation in the medium since a homogeneous medium without dislocations can only support a uniform stress field. One way in which an inhomogeneous stress field may form is by faulting under the influence of a high shear stress field, perhaps when the material is deep in the earth, and then removing the external shear stress by, for example, a gradual rise of the material to the earth's surface. The result is a stress concentration frozen into the material with a highly inhomogeneous stress field.

Nonuniform stress fields produce more complex effects. We analyze the body and surface waves when explosions occur near two types of stress concentrations — a point static dislocation and a center of compression both located two elastic radii from the explosion center. The results are similar for both cases. The stress field from a stress concentration varies as the inverse cube of the distance from the stress concentration, causing a strong variation in prestress across the shatter zone. If the stress concentration is near the direction of the body wave takeoff angle, there can be large effects on the explosion body waves. Surface waves, on the other hand, are affected only by the average stress field. A stress concentration which causes a prestress of about 100 bars at the cavity center (800 bars at maximum at the elastic radius) can generate surface waves and body waves comparable to the explosion surface and body waves. Note that this high stress field needs to exist only locally and at depth to cause body wave anomalies. A summary of the results of calculations for a number of configurations of stress concentrations near explosions is given in Table 3.4 and Figures 3.9 through 3.14.

While surface wave anomalies have been widely reported, reports of body wave anomalies are less common. However, since body waves are observed from only a small part of the focal sphere and may be strongly affected by travel path effects, body wave anomalies will generally be difficult to detect. A clear body wave anomaly

was observed from the explosion PILEDRIVER, however. In order to estimate what kinds of anomalies may be expected in Soviet explosions, we have constructed a model of the prestress field which could explain the PILEDRIVER anomalies.

The explosion PILEDRIVER had three anomalous features. It generated large Love waves, the Rayleigh waves had a pronounced radiation pattern with polarity reversals to the Northeast, and the body waves were greatly reduced in amplitude at stations to the Northeast. We can explain these facts simultaneously by assuming a strong compressional stress concentration to the Northeast of the explosion. A number of different types of stress fields could explain these observations, but it must be concentrated to the Northeast with a maximum stress of about a kilobar. Rayleigh wave reversals are caused by an inward motion (parallel to the surface) in this direction. Small body wave amplitudes occur near a node in the body wave radiation pattern. There are other possible explanations for the PILEDRIVER body wave anomalies. Hadley and Hart(1979) for example, suggested that the deep structure of the climax stock was responsible. The very large surface wave anomalies observed from this explosion, however, suggest the presence of a large tectonic stress field which could affect the body waves as well. Furthermore, recent stress measurements in the climax granite (Heuze, et al., 1980) found the nonhydrostatic stresses to be large and highly variable.

Tectonic strain release is one of the few mechanisms which can explain Rayleigh wave reversals. Massé (1981) reviews a number of hypotheses which have been made for this and other surface wave anomalies. A common explanation has been that the reversals are caused by spall slapdown following the explosion. However, Day, Rimer and Cherry (1981), show that if momentum is to be conserved, then spall cannot cause Rayleigh wave reversals and that spall has only minimal effects on surface wave amplitudes at periods longer than ten seconds. Similar problems arise with other passive mechanisms for producing Rayleigh wave reversals.

These results have importa t consequences for yield estimation and earthquake-explosion discrimination. It is possible for Rayleigh wave reversals to occur without affecting body wave amplitudes; however, the presence of surface wave anomalies increases the possibility of body wave anomalies. This introduces a bias into yield estimates which may be difficult to remove. Body waves may be amplified or reduced, or both, (at different receiving stations) by tectonic release although this effect is reduced to some extent by the fact that the explosion body wave and tectonic body wave are not exactly in phase, and so will not cancel completely at high frequencies. Clearly it is important to have as broad a coverage of the focal sphere as possible. In the case of PILEDRIVER, strong reductions in body wave amplitudes occurred over a limited range of azimuths, but our models show only a small effect on body wave amplitudes in other directions. This highly directional behavior is characteristic of stress concentrations.

A practical method for removing the effects of tectonic release would be to apply modern inverse theory techniques to the body and surface waves simultaneously. Our expansion in multipolar coefficients lends itself well to this type of analysis. In effect, this procedure would be an automated version of the trial and error method used here for PILEDRIVER which would consider all possible stress fields simultaneously. It should also be superior to commonly used moment t inversion schemes since we have an estimate of the frequency dependence of the composite source and are not restricted to a monopole plus double couple source.

The effect of tectonic release on discrimination is not as severe in most cases as the effect on yield estimates, especially if coverage is good. Although tectonic release adds an "earthquake-like" radiation pattern and reduces m_b (and M_s) in certain directions, the general effect is to add energy to the explosion body and surface waves. Since the explosion and tectonic body waves are more nearly in phase at longer periods, destructive interference will reduce the long period amplitude relative to the

short period amplitude. Furthermore, inhomogeneous prestress fields preferentially add high frequency energy which tends to increase the corner frequency. Since discrimination methods based on spectral analysis such as the Variable Frequency Magnitude method (e.g., Savino, Archambeau and Masso, 1980) compare a low frequency amplitude with a high frequency amplitude, both of these effects improve discrimination. Nevertheless, tectonic release can cause discrimination problems in some cases. Tensile stress fields, for example, may increase M_S significantly while leaving m_b unchanged, thus causing a more "earthquake-like" event.

It should be emphasized that in this report we have considered only tectonic release as the cause of anomalous radiation from explosions. We have done this in order to determine the nature and size of prestress fields necessary to cause the observed anomalies, not to rule out all other explanations. It is possible, for example, that the Rayleigh wave reversals from PILEDRIVER were due to tectonic release in a uniform stress field while the body wave anomaly was caused by a structural feature. Body wave anomalies, in general, do require much higher stresses than surface wave anomalies and uniform stress fields will not strongly affect body waves. Nevertheless, we find nothing inconsistent with the hypothesis that stress concentrations may exist and cause variations in body wave amplitudes such as those observed from PILEDRIVER. This must therefore be considered as a possible source of bias in yield estimates.

II. A MODEL FOR SEISMIC RADIATION FROM AN EXPLOSION IN A PRESTRESSED MEDIUM

Almost all nuclear explosions generate some "anomalous" radiation in the form of Love waves and nonisotropic Rayleigh waves (e.g. Toksöz and Kehrer, 1972). In some cases, however, the anomalous effects can be very large and actually dominate the observations. There are a number of possible explanations for this including release of tectonic prestress, anisotropy of the medium, nonsphericity of the source, near source scattering, slippage on joints and faults, and induced earthquakes. An excellent review of the subject can be found in a recent paper by Masse (1981). All of these mechanisms will cause the generation of some shear waves and cause nonisotropic radiation patterns. It is difficult, however, to explain the large anomalies of FILEDRIVER and other explosions in which the Rayleigh waves actually reverse polarity. Since the "anomalous" source must actually exceed the direct source at long periods, it seems unlikely to result from a passive effect such as scattering or slippage on joints and faults. Tectonic release can explain Rayleigh wave reversals since it adds energy to the explosion from energy stored in the earth.

Hadley and Hart (1979) pointed out that the body waves from PILEDRIVER were anomalous as well as the surface waves. In particular, the amplitudes were greatly reduced at observation points to the Northeast. Tectonic release from stress concentrations can cause this kind of variation in the body waves.

We use the following model for computing body and surface waves from an explosion in a prestressed medium. For the explosion, we consider two models. The first is the empirical model of Mueller and Murphy (1971) in which the explosion is described by a pressure pulse of the form:

$$P(t) = (P_0 e^{-\alpha t} + P_{0c}) H(t)$$

applied at the elastic radius (the point beyond which motion is elastic). The constants P_0, α, P_{0c} are determined empirically

and are functions of yield, material properties and source depth. For PILEDRIVER with a yield of 60 kilotons and a depth of 470 meters in granite, these constants are P_o = 130 bars, P_{oc} = 50 bars, α = 15 sec^{-1}. The elastic radius is 725 meters. In the second source model, a finite difference calculation is performed for the explosion to determine the reduced velocity potential which is then used to synthesize body and surface waves (Model No. 469 from Bache, Barker, Rimer, and Cherry, 1980). The elastic radius for the PILEDRIVER finite difference calculation is 870 meters.

The seismic radiation from tectonic release is modeled using the solution of Stevens (1980) for the sudden creation of a spherical cavity in a prestressed medium. This solution is reviewed in Appendix 1. By "cavity" we mean a region in which all material strength is lost. The density may remain constant. A problem with this model is how to determine the effective cavity radius. Tectonic stress will be released thoughout a region in which a substantial amount of cracking occurs. This region will be considerably larger than the explosion cavity. On the other hand, it must be smaller than the elastic radius. For the purposes of this study, we take the effective "cavity radius" to be equal to the elastic radius. The numbers we find will therefore be the lower limit of the actual prestress field. A smaller cavity radius will require a larger prestress field for the same effect. The scaling relations are derived in Appendix 4. It is approximately true that the generation of seismic waves varies as the product of the stress field and the cube of the radius. A factor of two decrease in radius requires a factor of eight increase in stress field to produce seismic waves of the same amplitude. This is not necessarily true for body waves, however, because of the complexity of the spectrum at short periods.

We can solve for the seismic radiation from a prestressed shatter zone for any prestress field (in a uniform whole space) by performing an expansion of the field in vector spherical harmonics. In Appendix 2 we derive the expansions for all uniform stress fields

and for two types of stress concentrations — a point center of compression and a point (static) dislocation.

We can make synthetic body waves and surface waves from these complex sources by reducing the vector solutions to scalar potentials. This conversion is given in Appendix 3. The potential solutions can be expanded in cylindrical potentials and incorporated in layered space codes using the method of Bache and Harkrider (1976) for body waves, and the method of Harkrider and Archambeau (1982) and Harkrider (1964) for surface waves.

Bache (1976) did a study of the effects of tectonic release on P-waves using the theory of Archambeau (1972) for the tectonic source. He concluded that tectonic release has a negligible effect on the body waves. Archambeau's theory was valid only for uniform stress fields, however. Using this model, Bache concluded that tectonic release could not have a significant effect on body waves without generating much larger surface waves than are observed and without assuming much higher stresses than seemed reasonable. The situation changes, however, when inhomogeneous stress fields and stress concentrations are considered. The following analysis will show that concentrated prestress fields can affect body waves more than surface waves. It is still true that stresses must be large, but they need only be large locally.

As shown in Appendix 1, the displacement field for the tectonic source can always be written in the form:

$$\underset{\sim}{u}(\underset{\sim}{x},\omega) = \sum_{\ell=0}^{\infty} \sum_{m=-\ell}^{\ell} \alpha_{\ell m}(\omega)\, \underset{\sim}{M}_{\ell m}(\omega,x) + s_{\ell m}(\omega)\, \underset{\sim}{N}_{\ell m}(\omega,\underset{\sim}{x})$$

$$+ \gamma_{\ell m}(\omega)\, \underset{\sim}{L}_{\ell m}(\omega,\underset{\sim}{x})$$

The coefficents $\alpha_{\ell m}$, $s_{\ell m}$, $\gamma_{\ell m}$ depend on the cavity size and type of prestress. The eignenvectors $\underset{\sim}{M}_{\ell m}$, $\underset{\sim}{N}_{\ell m}$, $\underset{\sim}{L}_{\ell m}$ represent toroidal, spheroidal shear, and spheroidal compressional waves respectively. In the far field these vectors become:

$$\underset{\sim}{M}_{\ell m}(\omega, \underset{\sim}{x}) = i^{\ell+1} \frac{e^{-K_\beta r}}{K_\beta r} \sqrt{\ell(\ell+1)}\ \underset{\sim}{C}_{\ell m}(\theta, \phi)$$

$$\underset{\sim}{N}_{\ell m}(\omega, \underset{\sim}{x}) = i^{\ell} \frac{e^{-iK_\beta r}}{K_\beta r} \sqrt{\ell(\ell+1)}\ \underset{\sim}{B}_{\ell m}(\theta, \phi)$$

$$\underset{\sim}{L}_{\ell m}(\omega, \underset{\sim}{x}) = i^{\ell} \frac{e^{-K_\alpha r}}{K_\alpha r}\ \underset{\sim}{P}_{\ell m}(\theta, \phi)$$

where the vectors $\underset{\sim}{P}_{\ell m}$, $\underset{\sim}{B}_{\ell m}$, $\underset{\sim}{C}_{\ell m}$ are defined in Appendix 1 and depend only on the observation coordinates θ, ϕ.

The far field displacement spectrum therefore consists of sums of terms of the form $\alpha_{\ell m}(\omega)/\omega$, $\beta_{\ell m}(\omega)/\omega$, $\gamma_{\ell m}(\omega)/\omega$ multiplied by angular and propagation factors. At high frequencies the spectra all fall off as ω^{-2}. At low frequencies, the function $\alpha_{\ell m}(\omega)/\omega$ falls off as $\omega^{\ell-1}$. The functions $\beta_{\ell m}(\omega)/\omega$, $\gamma_{\ell m}(\omega)/\omega$ are combinations of two functions which fall off as ω and $\omega^{\ell-2}$ at low frequencies. Thus for $\ell > 2$ all coefficients vanish in the limit $\omega \to 0$. At sufficiently low frequencies, any source must therefore look like a monopole plus a quadrupole. No matter how complex the source, the long period surface waves must look very nearly like an explosion plus a double couple.

For uniform stress fields, only $\ell=2$ and $\ell=0$ terms exist. For nonuniform stress fields, however, the higher order terms exist. These terms vanish at low frequencies and peak at higher frequency with increasing ℓ. The frequency of the peak is given approximately by $F_{max} = \ell V/2\pi R$ for SH waves and by $(\ell+1)V/2\pi R$ and $(\ell-1)V/2\pi R$ for the two P-SV waves mentioned before where V is the appropriate wave velocity. Inhomogeneous stress fields can therefore cause much larger variations in the body waves than in the surface waves, especially for large explosions. Higher order terms will be important when $V/2\pi R \leq f_o$ where f_o is the dominant frequency of the recording instrument. For PILEDRIVER, this ratio is about 1 Hz. In addition to adding high frequency energy, the

higher order multipoles have a more complicated variation with angle so inhomogeneous stress fields can give highly directional variations in body waves.

In Appendix 2 we derive the multipole coefficients for two types of stress concentrations. In the following section we will compute synthetic seismograms and body and surface wave radiation patterns using these sources. As a general rule, if one part of the "cavity" is more highly prestressed than another, larger amplitude tectonic body waves will be generated in the direction of the higher prestress. Depending on the sign of the prestress, the explosion body waves will be either amplified or reduced in this direction. Surface waves, on the other hand, will be sensitive only to the average stress field on the surface.

III. THE EFFECTS OF HOMOGENEOUS AND INHOMOGENEOUS PRESTRESS FIELDS ON SURFACE AND BODY WAVES

In this section we make a quantitative comparison of the effects of different types of prestress fields on body and surface waves. We have synthesized seismograms from a number of different prestress fields and made amplitude comparisons and radiation patterns for each.

Our purpose in this section is to make estimates of the effect of tectonic release and the magnitude of the prestress necessary to cause significant changes to the explosion seismic waves. We have used earth models appropriate for PILEDRIVER in all our calculations. The results, however, are not very sensitive to the structure and should be applicable to most regions of the earth. The structures used are given in Tables 3.1 and 3.2. For the body waves, the source region is a PILEDRIVER climax stock model (after Bache et. al., 1975). The receiver structure is a standard Eastern United States receiver structure. For surface waves, we used the PILEDRIVER structure over the Eastern United States model S1 of Bache, Swanger and Shkoller (1980). The body wave calculation used $t^* = 0.8$. The body wave synthetics were made using a WWSSN short period instrument response. The upgoing body waves were reduced by half to account approximately for near surface attenuation at one hertz. The surface wave synthetics were made through an LRSM long period instrument. All synthetics were made using a cavity radius equal to the Mueller-Murphy elastic radius of 725 meters. This is somewhat smaller than the finite difference elastic radius of 870 meters. The receiver point was taken to be at a distance of 4000 kilometers. This requires a takeoff angle of 28 degrees for the body waves. The Rayleigh and Love wave synthetics include only the fundamental mode.

Synthetic seismograms for the explosion source are shown in Figure 3.1. In this and the following figures, the body waves are normalized to the amplitude of the Mueller-Murpny explosion body wave. Surface (Rayleigh and Love) waves are normalized to the

TABLE 3.1

CRUSTAL MODELS FOR BODY WAVE CALCULATIONS

Depth (Km)	Thickness (Km)	α (Km/sec)	β (Km/sec)	ρ (gm/cm^3)
		SOURCE REGION		
.05	.05	1.50	1.00	1.50
.10	.05	4.50	2.65	2.55
2.00	1.90	5.33	3.15	2.67
4.00	2.00	5.90	3.25	2.70
∞	∞	6.00	3.30	2.80
		RECEIVER REGION		
.6	.6	3.70	2.16	2.10
2.6	2.0	4.55	2.54	2.20
4.0	1.4	5.60	3.14	2.65
5.0	1.0	6.00	3.30	2.80

TABLE 3.2

CRUSTAL MODEL FOR SURFACE WAVE CALCULATIONS

Depth	Thickness	α	β	ρ	Q
.05	.05	1.5	1.0	1.5	10
.10	.05	4.5	2.65	2.55	20
2.00	1.90	5.33	3.15	2.67	200
4.00	2.00	5.90	3.25	2.70	300
6.20	2.20	6.10	3.30	2.85	400
13.20	7.00	6.30	3.40	2.94	1200
19.00	5.80	6.40	3.45	3.00	1500
35.00	16.00	6.60	3.60	3.09	2000
∞	∞	8.10	4.50	3.35	2000

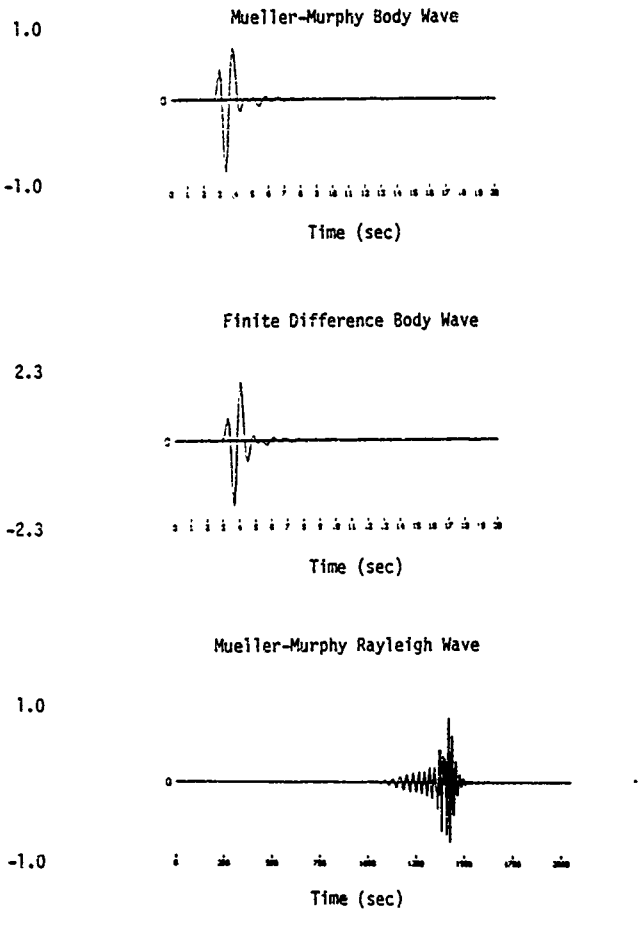

Figure 3.1. Synthetic seismograms for explosion sources without tectonic release. Top is Mueller-Murphy empirical body wave source synthetic. Middle is body wave from Finite Difference Calculation of reduced velocity potential. Bottom is synthetic Rayleigh wave from the Mueller-Murphy source.

Mueller-Murphy Rayleigh wave. For comparison, the finite difference body waves are shown. They are similar in shape with a slightly larger overshoot at the end because of the higher frequency content in the finite difference source. The body wave amplitude is greater by a factor of 2.3. The surface waves are identical in shape, but lower in amplitude by a factor of 0.8.

3.1 HOMOGENEOUS STRESS FIELDS

We first want to show the effects of tectonic release from explosions in spatially uniform stress fields with different orientations. Figure 3.2 shows the body and surface wave synthetic seismograms for a uniform σ_{12} stress field of one bar in which a spherical cavity is suddenly formed. The radiation pattern from this source is equivalent to a strike slip double couple (with a strike of -90°). The body waves are very similar to the body waves from the explosion. The main difference is a slight broadening of the waveform (and a change in sign at this azimuth). The surface waves in these and all of the following examples except for the σ_{13} stress field are identical except for changes in sign. The sources are small enough that the surface waves seen through a long period instrument are insensitive to source properties other than the seismic moment.

Figures 3.4 to 3.7 show the body and surface wave radiation patterns for a number of different uniform stress fields. The coordinates used are shown in Figure 3.3. The results are summarized in Table 3.3. The numbers shown are the amplitudes relative to the Mueller-Murphy PILEDRIVER source for a unit prestress. The shaded regions are the regions where the sign of the wave is reversed relative to the explosion. For surface waves, this is a well-defined region. For body waves, it is less well-defined since the waveforms can vary in shape as well as in sign, especially near nodes.

The σ_{12} (Figure 3.4) stress field causes a four lobed pattern of body and surface waves. This stress field is much more efficient at generating surface waves than body waves. (Body waves

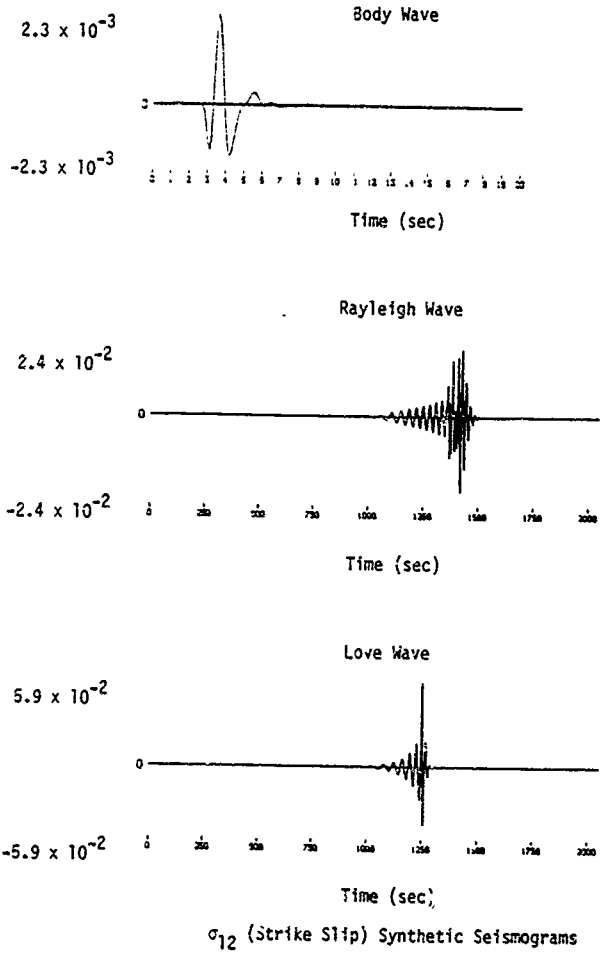

σ_{12} (Strike Slip) Synthetic Seismograms

Figure 3.2. Synthetic seismograms from tectonic release in a σ_{12} stress field. The three seismograms are the P-wave, Rayleigh wave and Love wave respectively. The shape of the Rayleigh and Love waves is nearly independent of the source and is very similar for all of the following examples.

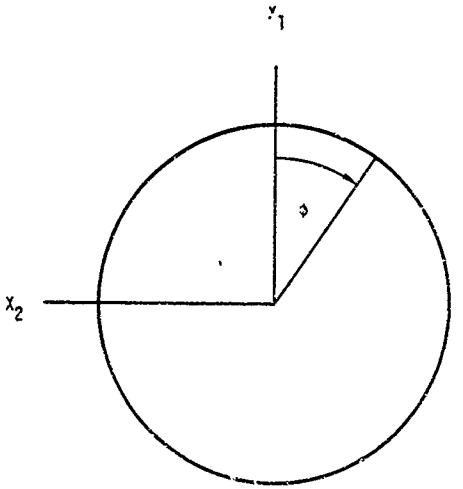

Figure 3.3. Coordinate systems used for calculations of synthetic seismograms and radiation patterns. The X_3 axis is out of the paper. The X_1 axis is taken to be $\phi = 0$ and North.

TABLE 3.3

BODY AND SURFACE WAVE AMPLITUDES FOR
EXPLOSIONS AND HOMOGENEOUS STRESS FIELDS

Source Type	P (28° takeoff)	Rayleigh	Love
EXPLOSION			
Mueller-Murphy (R=725m)	1.0	1.0	0.0
Finite Difference (R=870m)	2.3	.80	0.0
UNIFORM STRESS FIELDS (bars) R=725m			
$\sigma_{12} = 1$ (strike slip)	$\pm\frac{1}{440}$	$\pm\frac{1}{42}$	$\frac{1}{17}$
$\sigma_{33} = 1$, $\sigma_{11} = -1$ (45° Thrust)	$\frac{1}{150}$	$-\frac{1}{32}$	$\frac{1}{35}$
$\sigma_{11} = -1$ (Uniaxial)	$-\frac{1}{325}$	$-\frac{1}{42}$	$\frac{1}{35}$
$\sigma_{13} = 1$ (Vertical Dip Slip)	$\pm\frac{1}{106}$	$\pm\frac{1}{800}$	$\frac{1}{1000}$
$\sigma_{11} = -1$ $\sigma_{22} = -1$, $\sigma_{33} = 2$ (cylindrical)	$+\frac{1}{85}$	$-\frac{1}{24}$	0

σ_{12} = 1 Bar

Strike Slip Equivalent

Maximum Amplitudes:

Body = .0023

Rayleigh = .024

Love = .059

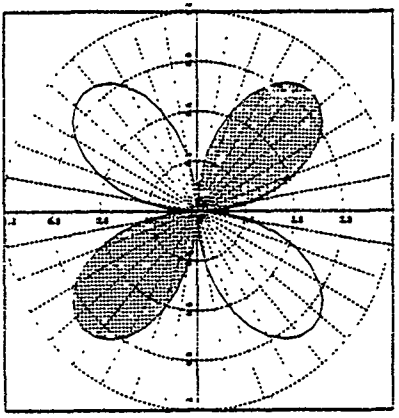

BODY WAVE

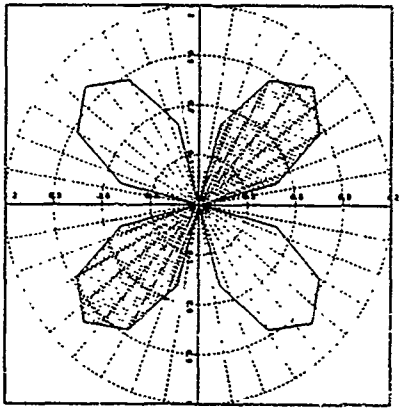

RAYLEIGH WAVE

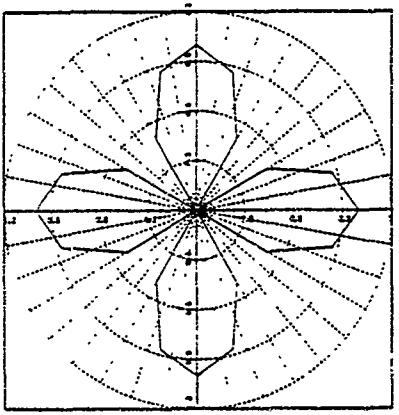

LOVE WAVE

Figure 3.4. Radiation patterns for body and surface waves for a σ_{12} uniform prestress field. Shaded areas indicate polarity opposite to the explosion in this and following figures. Amplitudes are relative to the Mueller-Murphy explosion source. Love and Rayleigh wave amplitudes are normalized to the explosion Rayleigh wave. Body waves are calculated at one hertz and have a 28 degree takeoff angle. Surface wave amplitudes are computed at 20 seconds.

$\sigma_{33} = 1$, $\sigma_{11} = -1$ (Bar)

45° Thrust Equivalent

Maximum Amplitudes:

Body = .0067

Rayleigh = .031

Love = .029

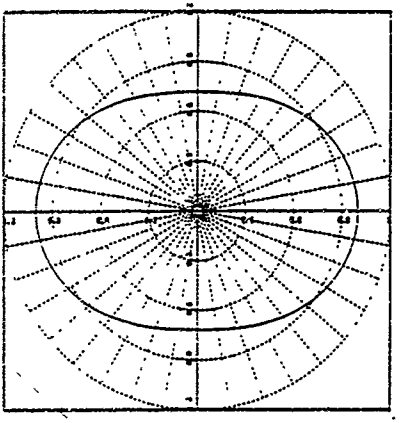

BODY WAVE

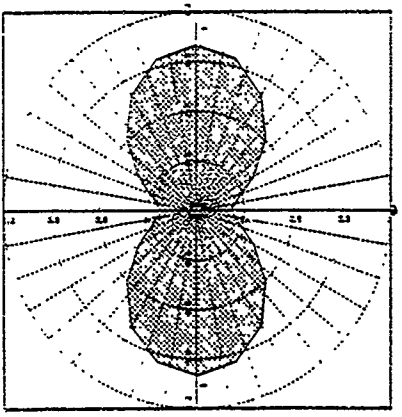

RAYLEIGH WAVE

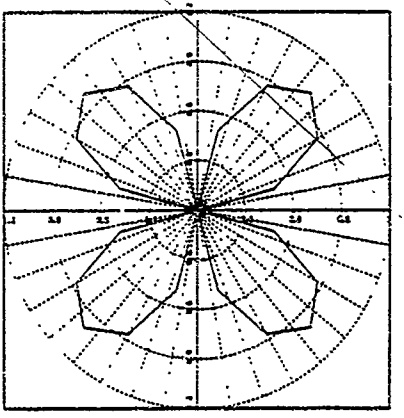

LOVE WAVE

Figure 3.5. Radiation patterns for $\sigma_{33} = -\sigma_{11}$ uniform prestress field.

σ_{11} = -1 Bar

Uniaxial Compression

Maximum Amplitudes:

Body = .0030

Rayleigh = .024

Love = .029

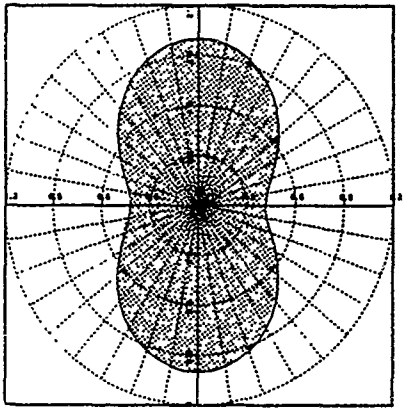

BODY WAVE

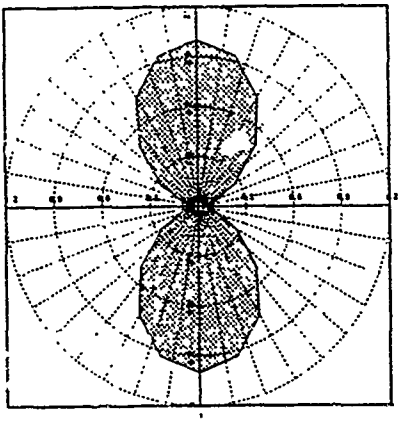

RAYLEIGH WAVE

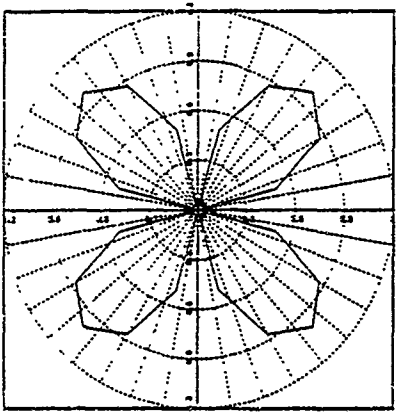

LOVE WAVE

Figure 3.6. Radiation patterns for uniaxial (σ_{11}) compression.

σ_{13} = 1 Bar

Vertical Dip Slip Equivalent

Maximum Amplitudes

Body = .0094

Rayleigh = .0012

Love = .0010

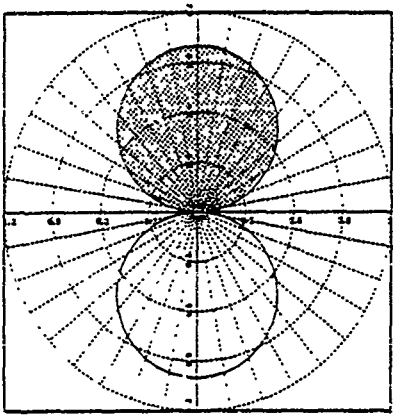

BODY WAVE

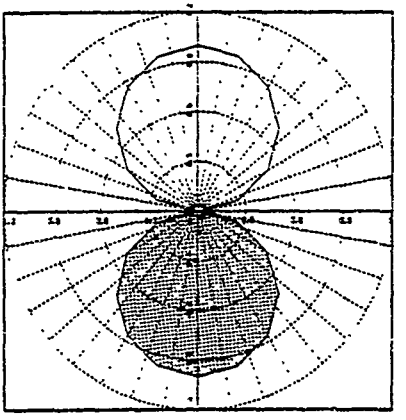

RAYLEIGH WAVE

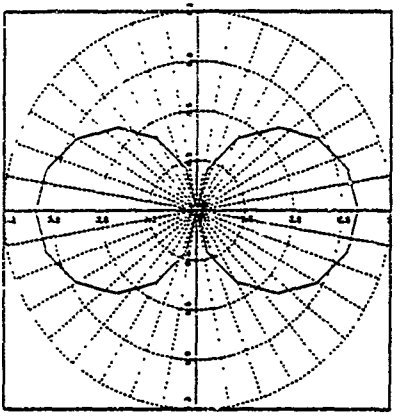

LOVE WAVE

Figure 3.7. Radiation patterns for σ_{13} uniform prestress field.

are observed near a node in the radiation pattern). The Rayleigh waves will be equal to the explosion Rayleigh waves with a prestress of 42 bars. Thus, Rayleigh waves will be phase reversed when the prestress exceeds 42 bars. Love waves will have more than twice the amplitude of the Rayleigh waves. Body waves, on the other hand, will equal the explosion body waves with a much higher prestress of 440 bars.

Figure 3.5 shows the body and surface wave radiation patterns for a stress field of $\sigma_{11} = -1$, $\sigma_{33} = 1$. This is equivalent to a 45 degree thrust fault (radiation pattern). This stress orientation is somewhat more efficient at generating body waves. It still requires a stress of 150 bars, however, to equal the explosion body wave. The explosion body waves are amplified at all azimutns. The tectonic Rayleigh waves are very large for this orientation, requiring a stress field of only 32 bars to equal the explosion Rayleigh wave. The Rayleigh waves are reversed at all azimuths for this stress field. Love waves, again, have a four-lobed pattern and have about the same amplitude as the Rayleigh waves.

Figure 3.6 shows the radiation pattern for uniaxial compression ($\sigma_{11} = -1$). This is similar to the 45 degree thrust orientation except for the lack of the vertical tensile component. The equivalent source is a 45 degree thrust plus an isotropic compression. This stress field causes a reduction in the body waves and a reduction (or reversal) of the Rayleigh waves at all azimuths. Again, the change in body waves is fairly small, requiring 325 bars to equal the explosion. Rayleigh wave reversals require a prestress about 40 bars and Love waves are about the same amplitude as Rayleigh waves. It would be difficult to distinguish these two cases observationally.

Figure 3.7 shows the radiation patterns for a σ_{13} stress field. This is equivalent to a vertical dip slip double couple. This orientation generates very small Love and Rayleigh waves with different frequency content than the other stress orientations. It is, however, a fairly good generator of body waves, requiring about

100 bars to equal the explosion P wave. The body waves have two lobes causing amplification in half the directions and reduction in the rest. This type of stress field can have an unpredictable effect on m_b-M_s ratios. Depending on the direction of the observation points, it could cause either an increase or a decrease in m_b without affecting M_s. The body wave generation of the dip slip and 45 degree thrust prestress orientations is a fairly strong function of takeoff angle varying as sin 2θ for the vertical dip slip and cos 2θ for the 45 degree thrust. The amplitudes become equal at θ = 22.5 degrees.

Because of the boundary condition of vanishing shear and normal tractions at the free surface, uniform σ_{13} and σ_{33} stress fields cannot exist; so the examples for "vertical dip slip" and "45 degree thrust" orientations are not physically possible. These may exist, however, as the lowest order terms of an inhomogeneous stress field. The radiation from tectonic release will then look like the radiation from one of these "forbidden" homogeneous prestress fields at sufficiently long periods. Also, an apparent σ_{33} stress field appears when the isotropic component is subtracted out from a uniaxial or cylindrically symmetric stress field.

3.2 INHOMOGENEOUS STRESS FIELDS

We next want to demonstrate the effects of stress concentrations on body and surface wave radation patterns. The results are summarized in Table 3.4. The body wave radiation patterns are for a frequency of one hertz and are for far field infinite space (no reflections) P-waves. The surface wave radiation patterns are for 20 second Love and Rayleigh waves.

As our first example of a stress concentration, we use a fairly simple source — a center of compression located one radius from the surface of the explosion shatter zone (Figure 3.8). The effect of this stress concentration is to cause a highly stressed region on a small part of the cavity surface. For the example chosen, the stress field is eight times larger at the surface of the

TABLE 3.4

BODY AND SURFACE WAVE AMPLITUDES
FOR INHOMOGENEOUS STRESS FIELDS

Angle – Stress Concentration to Down	Polarity	P	Rayleigh	Love
Center of Compression		$\frac{1}{91}$	$\frac{1}{64}$	$\frac{1}{104}$
30°	-	[150°, 30°]	none	
	+	none	all	
		$\frac{1}{104}$	$\frac{1}{76}$	$\frac{1}{46}$
45°	-	[190°, 350°]	[60°, 120°]	
	+	[80°, 100°]	[-60°, 60°]	
		$\frac{1}{152}$	$\frac{1}{64}$	$\frac{1}{31}$
60°	-	[220°, 320°]	[45°, 135°]	
	+	[0°, 180°]	-45°, 45°]	
		$\frac{1}{163}$	$\frac{1}{37}$	$\frac{1}{27}$
90°	-	none	[30°, 150°]	
	+	all	[-30°, 30°]	
Vertical Dip Slip Dislocation		$\frac{1}{183}$	$\frac{1}{58}$	$\frac{1}{27}$
45°	-	all	[40°, 140°]	
	+	none	[-40°, 40°]	

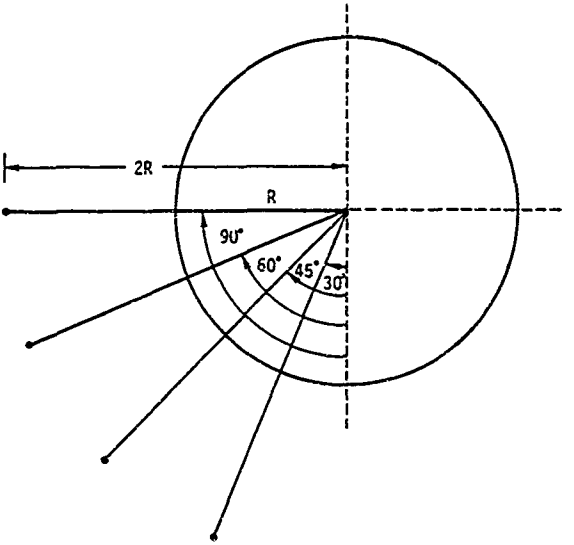

Figure 3.8. Location of stress concentration in examples.

cavity in the direction of the stress concentration than at the center. The stress field falls off with the cube of the distance from the center of compression. All of the examples are normalized to a stress of 1 bar at the cavity center.

The radiation patterns are quite sensitive to the location of the stress concentration; so we show a sequence of figures with radiation patterns from stress concentrations at different depths. Again, the shaded areas indicate reversal with respect to the explosion polarity. For body waves, as mentioned before, this is only approximate since both the phase and amplitude of the waves vary with angle. If the stress concentration is directly under the explosion, then the radiation is azimuthally symmetric. The body waves are all decreased in amplitude, the Rayleigh waves are increased in amplitude, and no Love waves are generated.

Figure 3.9 shows the body and surface wave radiation patterns for a stress concentration located 30 degrees from down (at an azimuth of minus 90 degrees on the figure). The tectonic body waves are reversed in polarity relative to the explosion at almost all azimuths, but the amplitude is much greater in the direction of the stress concentration than in other directions. The effect of this stress field when added to the explosion is to selectively reduce the body waves in this direction. It is also a good generator of body waves relative to surface waves. Ninety bars (at the center, 720 maximum) is required to cancel the explosion body wave although small phase differences forbid exact cancellation. Rayleigh waves would be amplified at all azimuths by this stress field. It is a better generator of Rayleigh waves than of Love waves.

Figure 3.10 shows the radiation patterns for a stress concentration 45 degrees from down. Again, the body waves are substantially reduced in the direction of the stress concentration. The Rayleigh waves are amplified in most directions; however, for a narrow range of azimuths in the direction of the stress concentration (and in the opposite direction), the Rayleigh waves are reversed. This stress field also generates large amplitude Love waves.

Stress Concentration at 30°

Maximum Amplitudes

Body = .011

Rayleigh = .015

Love = .010

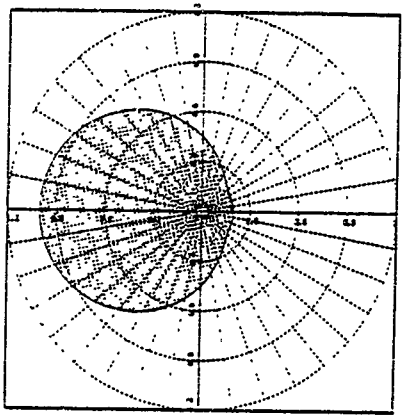

BODY WAVE

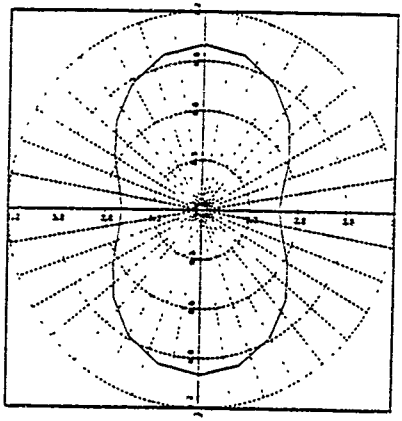

RAYLEIGH WAVE

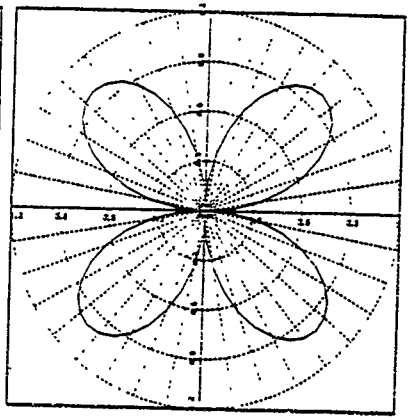

LOVE WAVE

Figure 3.9. Radiation patterns for tectonic release from a stress concentration located 30° from down.

Stress Concentration at 45°

Maximum Amplitudes

Body = .010

Rayleigh = .013

Love = .022

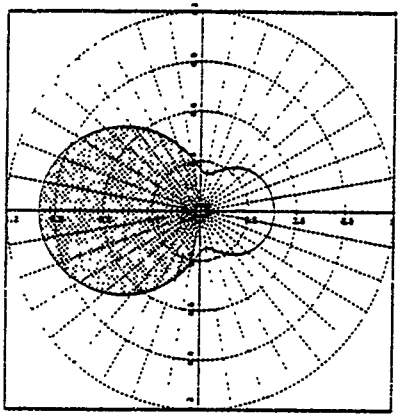

BODY WAVE

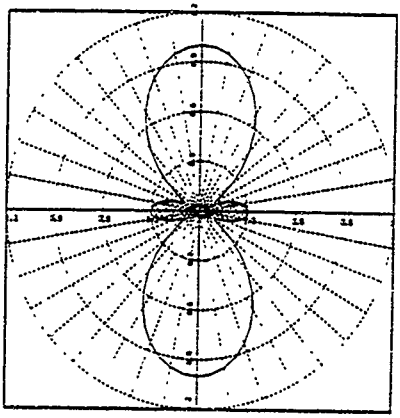

RAYLEIGH WAVE

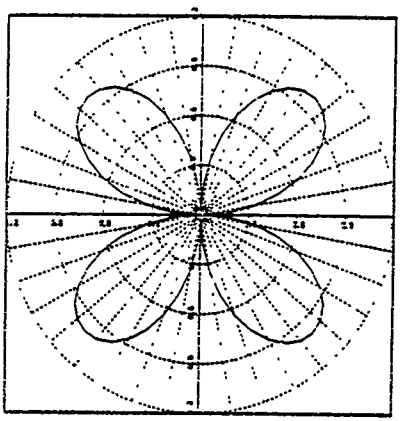

LOVE WAVE

Figure 3.10. Radiation patterns from a stress concentration at 45°.

Figure 3.11 shows the radiation pattern for a stress concentration located 60 degrees from down. This configuration still causes a body wave reduction in the direction of the stress concentration. It is less efficient than the previous examples, however, and directions away from the stress concentration see an amplification of the body waves. There is a large region in which Rayleigh waves are reversed. At some azimuths, they are amplified.

Figure 3.12 shows the radiation patterns for a stress concentration at 90 degrees at the same depth as the center of the cavity. Now body waves are amplified at all azimuths. Rayleigh waves are reversed at all but a narrow range of azimuths. This stress field is a relatively efficient generator of Love and Rayleigh waves.

Figure 3.13 shows synthetic seismograms at three observation points — azimuths of minus 90, 0, and 90 degrees with a center of compression at an azimuth of minus 90 degrees and 45 degrees from down (radiation pattern of Figure 3.10). At minus 90 degrees, the tectonic body wave has almost the same shape as the explosion and will therefore tend to reduce the body wave. At 90 degrees, the wave is amplified. At 0 degrees, the waveform is more complex and does not clearly increase or decrease the explosion body wave.

As a second example of a stress concentration, we use a point static dislocation located two radii from the cavity center. The dislocation is located at an azimuth of minus 90 degrees as with the center of compression examples. It has a vertical dip slip orientation and is located 45 degrees from down. The explosion then is in a compressive quadrant of the double couple radiation pattern. Again, the stress field falls off with the cube of the distance. The radiation patterns for this source are shown in Figure 3.14. The radiation resembles that of the center of compression. It is slightly more efficient at generating surface waves and slightly less efficient at generating body waves than the center of compression. The dislocation at 45 degrees has radiation patterns and amplitudes much like the center of compression at 60 degrees.

Stress Concentration at 60°

Maximum Amplitudes

Body = .0066

Rayleigh = .016

Love = .032

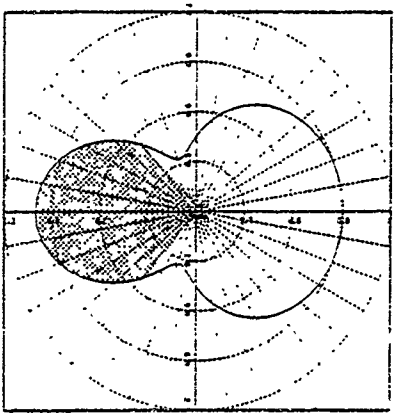

BODY WAVE

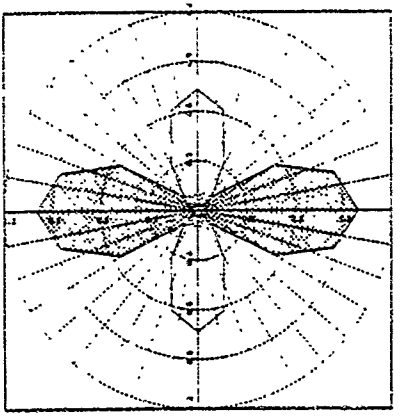

RAYLEIGH WAVE

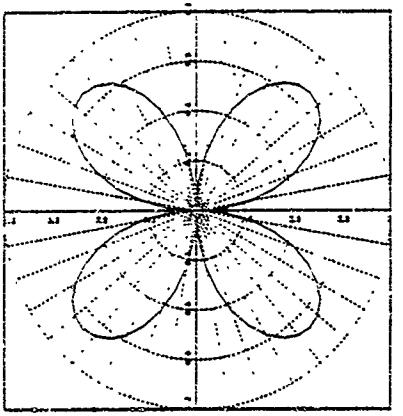

LOVE WAVE

Figure 3.11. Radiation patterns from a stress concentration at 60°.

Stress Concentration at 90°

Maximum Amplitudes

Body = .0060

Rayleigh = .027

Love = .037

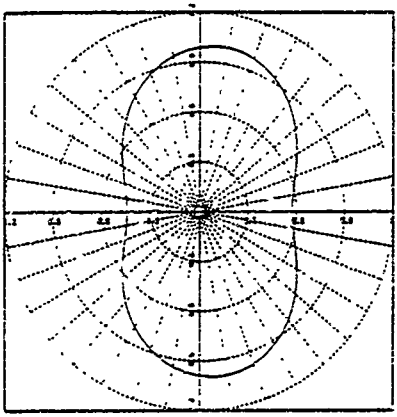

BODY WAVE

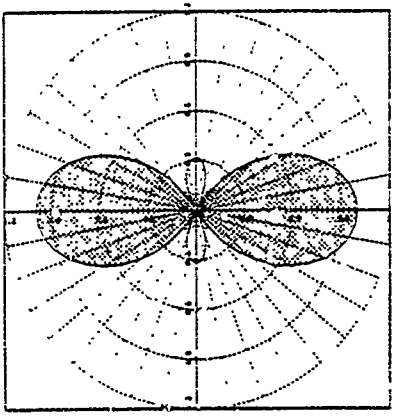

RAYLEIGH WAVE

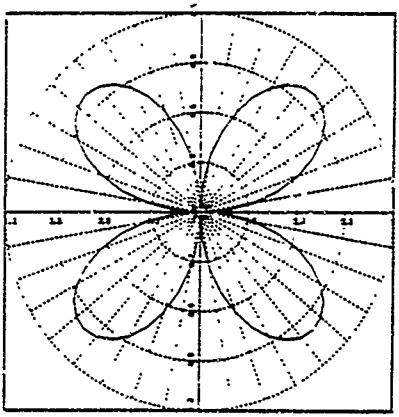

LOVE WAVE

Figure 12. Radiation patterns from a stress concentration at 90°.

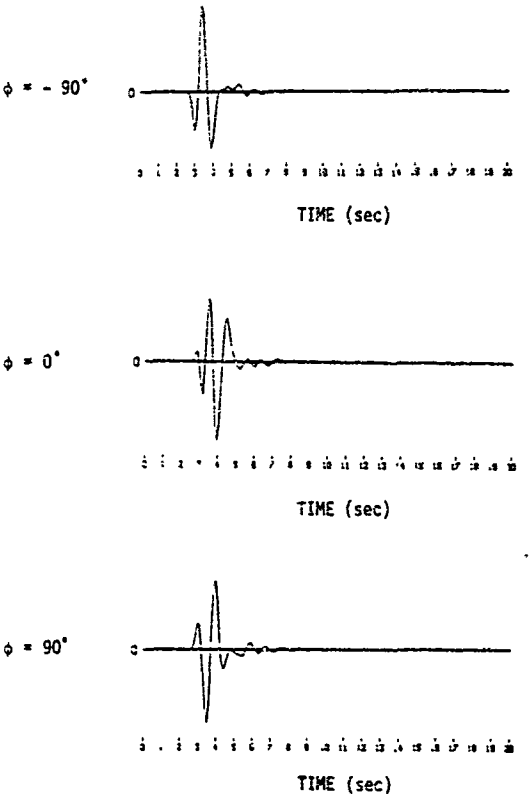

Figure 3.13. Synthetic body wave seismograms at different azimuths. The stress concentration is located 45° from down at $\phi = -90°$. The wave forms change in shape with azimuth and reduce the body wave in the direction of the stress concentration.

Vertical Dip Slip
Dislocation at 45°
Body = .006
Rayleigh = .017
Love = .037

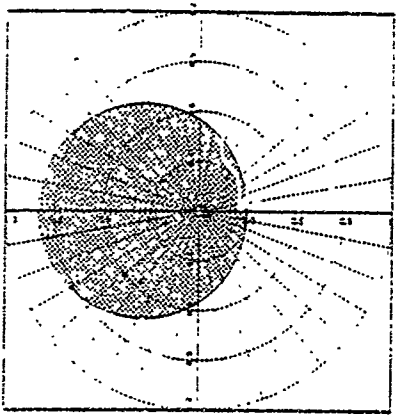

BODY WAVE

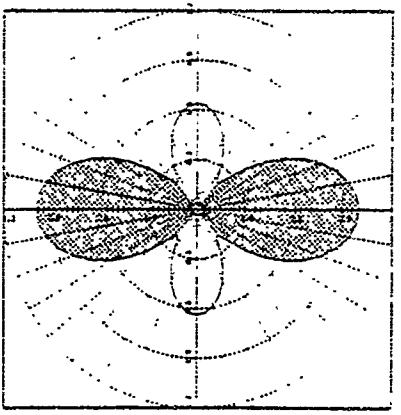

RAYLEIGH WAVE

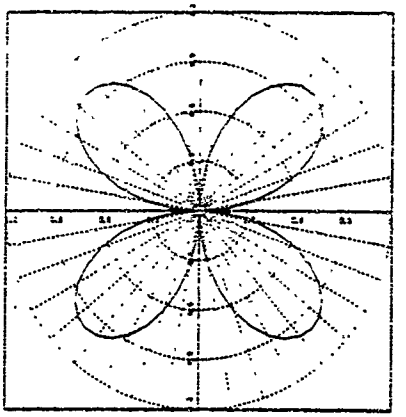

LOVE WAVE

Figure 3.14. Radiation patterns from a vertical dip slip static dislocation at 45°.

In the preceding example, notice that the stress field was caused by a vertical dip slip dislocation, but the radiation generated by tectonic release in this stress field is very different from that found previously for a "vertical dip slip" homogeneous prestress field. It is, in fact, very efficient at generating surface waves and has much the same effect as the stress field of the point center of compression.

It is clear from these examples that the relative effects of stress concentrations on body and surface waves is highly dependent on the location of the stress concentration. The body waves can have complex radiation patterns — patterns which could not occur with a simple double couple source. It is approximately true that the generation of body waves is a function of the distance from the stress concentration to the surface of the cavity (shatter zone) while the generation of surface waves is a function of the the distance from the stress concentration to the center of the cavity. The effect on body waves will therefore be stronger compared to the effect on surface waves if the stress concentration is moved closer to the explosion. This is especially true for large explosions. As pointed out in the last section, the higher order multipoles add in seismic energy at and above the corner frequency. If the corner frequency is much higher than the observation frequency, these effects will not be observed. At frequencies higher than the corner frequency, these effects will be very important. The effect on surface waves will usually be indistinguishable from a quadrupole plus isotropic source. Body waves will generally be increased in directions corresponding to tensile stresses on the sphere and decreased in directions of compressive stress on the sphere. The stresses necessary are higher than the stresses for uniform stress fields for body waves of the same amplitude. For example, with a center of compression at 45 degrees from down, it requires a maximum stress of 800 bars to equal the explosion body wave compare to 200 bars for a "45 degree thrust" stress orientation. This region of high stress is quite small, however, and decreases by a factor of 27 across the cavity.

IV. A TECTONIC SOURCE MODEL FOR PILEDRIVER

The explosion PILEDRIVER emitted highly anisotropic surface waves and body waves. Toksöz and Kenrer (1972) were able to match the Rayleigh wave radiation patterns with the superposition of a strike-slip double couple. In their model, the amplitude of the Rayleigh waves created by the double couple exceeded those of the explosion by a factor of 3.2. This number can be reduced by using a different orientation of the double couple such as a 45 degree thrust orientation, but it is still a very large effect. The observed Rayleigh wave polarity was reversed at azimuths to the Northeast.

Hadley and Hart (1979) compared the body waves from PILEDRIVER with the body waves from the explosion JORUM and found a substantial variation in the amplitude of the body waves with station azimuth. In particular, the body waves in the Northeasterly directions were reduced by as much as a factor of six. Table 4.1 shows the body wave amplitude data for JORUM and PILDERIVER and the ratio of the amplitudes scaled with the cube root of the yields. The data is from two Sierra Geophysics reports (Hadley, 1979, and Hadley and Hart, 1979).

The fact that the Rayleigh wave reversals are in the same direction as the body wave anomaly suggests that they both have the same cause. The purpose of this analysis is to assume that the anomalies are due to tectonic release and to see what magnitudes and orientations of stress fields are necessary to match the observations. The solution is not unique, but there are some strong constraints on the problem. Since the body wave variation is large, the prestress field cannot be too efficient at creating surface waves relative to body waves. A "strike-slip" (σ_{12}) prestress, for example, would generate very large surface waves without substantially affecting the body waves. A second constraint is that the Rayleigh waves are reversed and the body waves are reduced in the same direction. This means that the prestress must be

TABLE 4.1

BODY WAVE AMPLITUDES FOR EXPLOSIONS PILEDRIVER AND JORUM

Station	Distance (degrees)	Azimuth (degrees)	J-Amp (m_u)	P-Amp (mu)	Scaled PILEDRIVER / JORUM
SCP	30.0	71.2	823	69	.214
OGD	32.4	70.0	745	46	.158
COL	33.2	336.1	1074	343	.816
WES	34.7	67.0	468	34	.186
KIP	39.9	258.7	1097	548	1.28
KTG	56.8	23.7	594	91	.391
AKU	59.9	28.3	365	91	.637
NHA	61.6	134.8	422	171	1.04
ARE	68.2	133.1	1268	446	.898
TOL	81.3	46.0	685	91	.339
STU	81.7	32.9	251	69	.702
SHK	83.9	309.1	868	114	.335
NAT	86.1	99.8	548	183	.853

compressive over a large part of the focal sphere in the Northeasterly direction. A "45 degree thrust" stress field, for example, causes a reduction in the surface waves but an amplification of the body waves. In fact, the only "fault-like" uniform stress field which could satisfy these conditions is a "strike-slip" stress field oriented approximately North-South with a compressive lobe to the Northeast and then rotated down to the Northeast so that there is a larger effect on the body waves.

There is no reason to restrict ourselves to uniform stress fields. In fact, the stress field almost certainly increases with depth. The major observational restriction is that the stress field be large and compressive to the Northeast. We will therefore try to match the body and surface waves with a stress concentration in the lower Northeast quadrant. From the figures 3.9 to 3.14 the location of the compressional stress concentration can be determined. If the stress concentration is located too low (0-45 degrees from down) then there is a large effect on the body waves, but an actual amplification of the surface waves and no significant Rayleigh wave reversal. If the stress concentration is at the same depth as the center of the cavity (90 degrees from down), then the Rayleigh waves can be reversed, but there is no reduction in the body waves. At 60 degrees, however, the effect is right. The negative Rayleigh wave lobe is large enough to cause a reversal when superimposed on the explosion source. Body waves are reduced preferentially in the Northeasterly direction. The best linear combination with the Mueller-Murphy explosion source is a center of compression at 60 degrees from down at an azimuth of 35 degrees from North with a 200 bar stress field at the cavity center. This leads to a maximum prestress of 1.6 kilobars on the "cavity" surface.

The radiation patterns for this source are shown in Figure 4.1. The Rayleigh wave radiation pattern agrees very well with the data given by Toksöz and Kehrer (1972, p.150). In fact, the match is better than their fit with a superimposed strike-slip double couple.

Composite PILEDRIVER
Source-Explosion
Plus Stress Concentration
at 60° from down

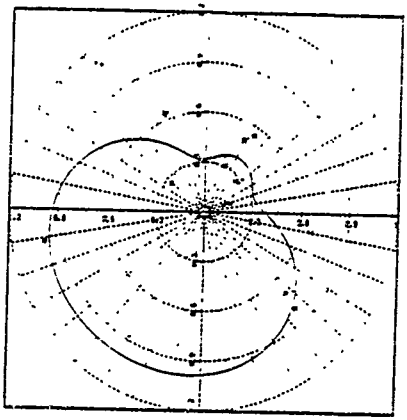

BODY WAVE

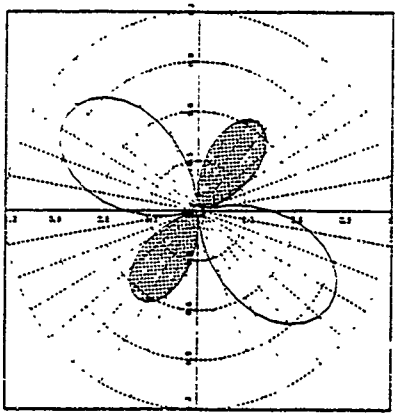

RAYLEIGH WAVE

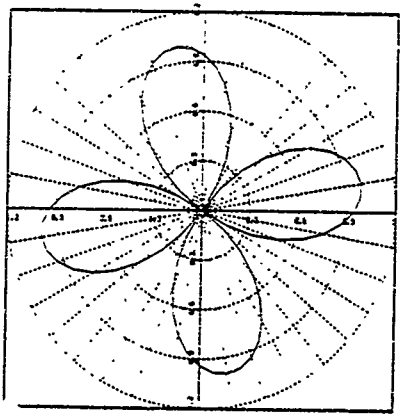

LOVE WAVE

Figure 4.1. Radiation patterns for composite PILEDRIVER source. Marks on body wave figure are PILEDRIVER observations divided by JORUM observations.

Rivers and Von Seggern (1981) did a moment tensor inversion for the PILEDRIVER source using Rayleigh waves and Love waves without restricting the "double couple" direction to be strike-slip. The Love wave radiation patterns for the resulting source are very similar to the Love wave patterns in Figure 4.1.

The body waves shown are for a frequency of 1 Hertz and a takeoff angle of 28 degrees. The data points shown are the amplitudes of PILEDRIVER divided by the amplitudes of JORUM at the stations listed in Table 4.1. The takeoff angles actually vary between 15 degrees and 30 degrees; so the stations farther away should have a more uniform radiation pattern than is shown on the figure. Agreement is quite good. The one bad datum is the low reading at station SHK (at azimuth of 310 degrees).

Figure 4.2 shows synthetic seismograms from the composite source along with their relative amplitudes. The conditions are the same as for the synthetics in the last section except that we used a value for t* of 1.05. This value was obtained by Bache, et al. (1975) for the path from NTS to Alaska. The observed amplitudes are close to the syntnetics. The Northeasterly waveforms are more complex due to interference of the explosion and tectonic body waves. The synthetic amplitude at OGD is too large indicating more complete destructive interference than is in our model.

Other types of stress concentrations to the Northeast give similar results. From the calculations in the last section, a vertical dip slip dislocation located 45 degrees from down has almost the same effect as the center of compression at 60 degrees. Again, with this source we can approximately match the surface and body waves. The maximum stress on the surface is about 1.5 kilobars.

As mentioned before, the maximum prestress on the cavity surface from point stress concentration is about 1500 bars. In fact, the stress field does not need to be this large. A somewhat more extended stress field can also cause the observed effects. Figure 4.3 shows the radiation patterns with a stress concentration at 45 degrees from down (maximum stress on cavity 800 bars) at an

Station	Amplitude	
KTG	Syn.	.36
	Obs.	.31
STU	Syn.	.45
	Obs.	.55
OGD	Syn.	.32
	Obs.	.13
ARE	Syn.	.73
	Obs.	.70
KIP	Syn.	1.0
	Obs.	1.0

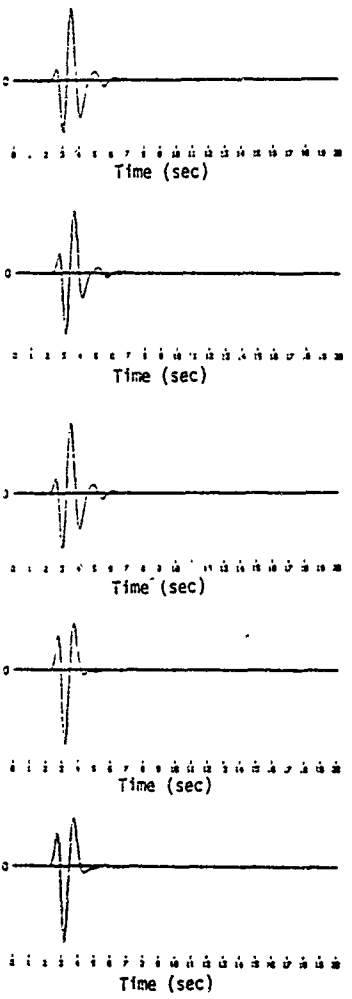

Figure 4.2. Body wave synthetic seismograms made using PILEDRIVER composite source. The complexity of the source causes a variation in waveform shape with takeoff angle and azimuth.

Composite PILEDRIVER
Source
Explosion Plus 100 Bar
Uniaxial Stress Plus
Stress concentration
at 45°

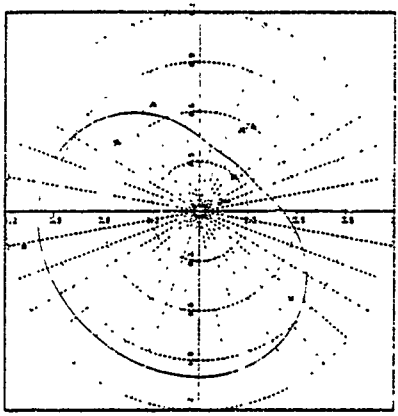

BODY WAVE

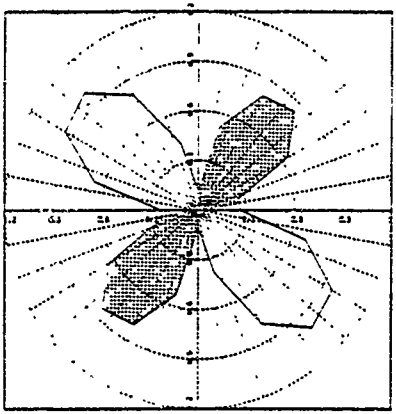

RAYLEIGH WAVE

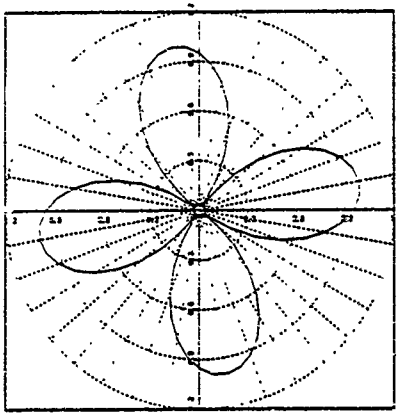

LOVE WAVE

Figure 4.3. Radiation patterns from second PILEDRIVER composite source.

azimuth of 40 degrees and a uniaxial prestress of 100 bars along the same azimuth. Again, the agreement is good, but the maximum stress field is only about 850 bars.

The crucial condition in this analysis is that the lower Northeast quadrant be under substantial compressive prestress. The surface waves are very insensitive to the type of prestress and are really only affected by the monopole and quadrupole components. The body waves are more sensitive to details of the stress field. From these examples it is obvious that we cannot determine the exact magnitude of the stress field. To within about a factor of two, however, the maximum stress should be approximately a kilobar. Furthermore, the stress needs to be high only locally and at some depth.

In this section we have demonstrated that the general features of the explosion PILEDRIVER — the Rayleigh wave reversals, large amplitude Love waves, and asymmetric body wave radiation pattern — can be explained if there is a compressive stress concentration of at least a kilobar to the Northeast of the explosion. We have not attempted to make a detailed model of the stress field or to explain small details of the seismograms. In principle, it should be possible to perform an inverse calculation to determine the multipole coefficients and the initial prestress field. This inversion could be done using body waves and surface waves simultaneously. The problem is, of course, under-determined since we have only limited coverage of the focal sphere, but would provide a method to describe the class of models which fit the data in a single calculation as opposed to using a trial and error method of forward modeling.

V. CONCLUSIONS AND RECOMMENDATIONS

Rayleigh wave reversals may be obtained if an explosion occurs in a medium with a prestress greater than about 50 bars, with the exact amount depending on the orientation of the stress field, assuming that the effective shatter zone radius is approximately equal to the elastic radius. The size of the effective radius is critical since the long period surface wave amplitude is proportional to the cube of the radius. The best way to determine the effective radius is by performing nonlinear calculations of explosions in prestressed media and comparing it with the linear result (Day, et al., 1981).

An important fact in light of recent observations is that the linear model used here does not produce time delays. Any time delays must result from tectonic release over an extended period of time. The only way to determine if time delays are present and the extent of these delays without making ad hoc assumptions is by performing full nonlinear calculations of explosions with tectonic release using realistic material models.

Surface waves are very insensitive to stress heterogeneity. Only the average stress field is important for long period Rayleigh wave excitation although the orientation of the average stress field is very important.

Explosions near stress concentrations may have significantly altered body waves. These effects can be strong in some cases and, in general, will be highly directional. Local stresses of about a kilobar are required to influence the body waves; however, these stresses need be this large only locally and at depths below the explosion. The average stress may be much lower than the local stress fields.

We have used the model for tectonic release to model the explosion PILEDRIVER. If the body and surface wave anomalies are due to tectonic release, then the observations require that the average stress field must be compressive in the northeast-southwest

direction. The body wave anomaly and surface wave anomaly can be explained simultaneously by a stress concentration below and to the northeast of the explosion.

Tectonic release causes problems for discrimination and yield estimation by causing variations in surface and body wave amplitudes at different locations. The most important step in removing these problems is to have as wide a coverage of stations as possible. Moment tensor inversion is a good way to remove the effects of tectonic release; however, a cylindrically symmetric stress field cannot be removed this way using surface waves alone.

VI. REFERENCES

Aki, K. and Y. Tsai (1972), "The Mechanism of Love Wave Excitation by Explosive Sources," JGR, 77, pp. 1452-1475.

Archambeau, C. B. (1972), "The Theory of Stress Wave Radiation from Explosions in Prestressed Media," Geophys. J. R. astr. Soc., 29, pp. 329-366.

Bache, T. C. (1976), "The Effect of Tectonic Release on Explosion P-Wave Signatures," BSSA, 66, pp. 1441-1457.

Bache, T. C. and D. G. Harkrider (1976), "The Body Waves Due to a General Seismic Source in a Layered Earth Model," BSSA, 66, pp. 1805-1819.

Bache, T. C., H. Swanger and B. Shkoller (1980), "Synthesis of Lg In Eastern United States Crustal Models with Frequency Independent Q," Systems, Science and Software Semi-Annual Technical Report to Advanced Research Projects Agency, SSS-R-81-4668, September.

Bache, T. C., T. G. Barker, T. R. Blake, D. G. Lambert, J. T. Cherry, J. M. Savino, and N. Rimer (1975), "An Explanation of the Relative Amplitudes of the Teleseismic Body Waves Generated by Explosions in Different Test Areas at NTS," Systems, Science and Software Final Report, SSS-R-76-2746, submitted to Defense Nuclear Agency, DNA 3958F, October.

Bache, T. C., T. G. Barker, N. Rimer and J. T. Cherry (1980), "Th Contribution of Two Dimensional Source Effects to the Far Field Seismic Signatures of Underground Nuclear Explosions," Systems, Science and Software Topical Report to Advanced Research Projects Agency, SSS-R-80-4569, July.

Ben-Menahem, A. and J. Singh (1968), "Eigenvector Expansions of Green's Dyads with Applications to Geophysical Theory," Geophys. J. R. astr. Soc., 16, pp. 417-452.

Cherry, J. T., N. Rimer and W. O. Wray (1975), "Seismic Coupling From a Nuclear Explosion: The Dependence of the Reduced Displacement Potential on the Nonlinear Behavior of the Near Source Rock Environment," Systems, Science and Software Technical Report to Advanced Research Projects Agency, SSS-R-76-2742, September.

Day, S. M., N. Rimer, and J. T. Cherry (1981), "Surface Waves from Underground Explosions with Spall: Analysis of Elastic and Nonlinear Source Models," Submitted to BSSA.

Day, S. M., N. Rimer, J. T. Cherry, and J. L. Stevens (1981), "The Shagan River Story (The Effects of Spall and Prestress on m_b and M_S)," Proceedings of VSC Research Conference, VELA Seismological Center Report VSC-TR-82-1, p. 63-68.

Goforth, T., B. Rafipour, and E. Herrin (1982), "Anomalous Rayleigh Waves from Nuclear Explosions at the USSR Shagan River Test Site," (to be submitted for publication).

Hadley, D. M. (1979), "Seismic Source Functions and Attenuation from Local and Teleseismic Observations of NTS Events JORUM and Handley," Sierra Geophysics Quarterly Technical Report to Advanced Research Projects Agency, SGI-R-79-002.

Hadley, D. M. and R. S. Hart (1979), "Seismic Studies of the Nevada Test Site," Sierra Geophysics Quarterly Technical Report to Advanced Research Projects Agency, SGI-R-79-003, June.

Harkrider, D. G. (1964), "Surface Waves in Multilayered Elastic Media I: Rayleigh and Love Waves from Buried Sources in a Multilayered Elastic Half-Space," BSSA, 54, pp. 627-679.

Harkrider, D. G. and C. B. Archambeau (1982), "Theoretical Rayleigh and Love Waves from an Explosion in Prestressed Source Regions," (in preparation).

Heuze, F. E., W. C. Patrick, R. V. de la Cruz, and C. F. Voss (1981), "In Situ Geomechanics: Climax Granite, Nevada Test Site," Lawrence Livermore Laboratory Report UCRL-53076, April.

Masse, R. P. (1981), "Review of Seismic Source Models for Underground Nuclear Explosions," BSSA, 71, pp. 1249-1268.

Morse, P. M. and H. Feshback (1953), Methods of Theoretical Physics, McGraw-Hill, New York.

Mueller, R. A. and J. R. Murphy (1971), "Seismic Characteristics of Underground Nuclear Detonations," BSSA, 61, pp. 1675-1692.

Patton, H. T. (1980), "Surface-Wave Generation by Underground Nuclear Explosions Releasing Tectonic Strain," Lawrence Livermore Report, UCRL-93062.

Rimer, N., J. T. Cherry, S. M. Day, T. C. Bache, J. R. Murphy, and A. Maewal (1979), "Two-Dimensional Calculation of PILEDRIVER, Analytic Continuation of Finite Difference Source Calculations, Analysis of Free Field Data from Merlin and Summary of Current Research," Systems, Science and Software Quarterly Technical Report to Advanced Research Projects Agency, SSS-R-79-4121, August.

Rivers, W. and D. N. Von Seggern (1981), "Effect of Tectonic Strain Release on Surface-Wave Magnitudes," to be published in Teledyne-Geotech Report.

Rygg, E. (1979), "Anomalous Surface Waves from Underground Explosions," BSSA, 69, pp. 1995-2002.

Savino, J. M., C. B. Archambeau, and J. F. Masso (1980), "VFM Discrimination Results from a Ten Station Network," Systems, Science and Software Technical Report submitted to VELA Seismological Center, SSS-R-80-4566, July.

Stevens, J. L. (1980), "Seismic Radiation from the Sudden Creation of a Spherical Cavity in an Arbitrarily Prestressed Elastic Medium," Geophys. J. R. astr. Soc., 61, pp. 303-328.

Stevens, J. L. (1982), "The Growing Spherical Seismic Source," Geophys. J. R. astr. Soc., 69, pp. 121-135.

Toksöz, N. and H. Kehrer (1972), "Tectonic Strain Release by Explosions and Its Effect on Discrimination," Geophys. J. R. astr. Soc., 31, pp. 141-161.

APPENDIX 1

SOLUTION FOR THE CREATION OF A SPHERICAL CAVITY IN A PRESTRESSED MEDIUM

APPENDIX 1

SOLUTION FOR THE CREATION OF A SPHERICAL CAVITY IN A PRESTRESSED MEDIUM

An integral equation for the displacement field caused by tractions $\underset{\approx}{T}(\underset{\sim}{u})\cdot\hat{n}$ applied to the inside of a cavity of any shape can be written (in the frequency domain) as:

$$\underset{\sim}{u}(\underset{\sim}{x}, \omega) = \int_{\Sigma} \underset{\sim}{u} \cdot \underset{\approx}{T}(\underset{\approx}{G}) \cdot \hat{n} dA - \int_{\Sigma} \underset{\approx}{G} \cdot \underset{\approx}{T}(\underset{\sim}{u}) \cdot \hat{n} dA \qquad (1)$$

where $\underset{\approx}{G}(\underset{\sim}{x}, \underset{\sim}{x}_0, \omega)$ is any frequency domain elastic Green's tensor, and Σ is the cavity surface. If the cavity is created suddenly in a prestressed medium, the apparent tractions are

$$\underset{\approx}{T}(\underset{\sim}{u}) \cdot \hat{n} = -\frac{1}{i\omega} \underset{\approx}{T}(\underset{\sim}{u}^*) \cdot \hat{n}$$

where $\underset{\approx}{T}(\underset{\sim}{u}^*)$ is the initial prestress.

For a spherical cavity equation (1) is separable. We define the complete set of vector spherical harmonics (after Ben-Menahem and Singh, 1968):

$$\underset{\sim}{P}_{\ell m} = \hat{e}_r Y_{\ell m}(\theta, \phi)$$

$$\sqrt{\ell(\ell+1)}\ \underset{\sim}{B}_{\ell m} = \left[\hat{e}_\theta \frac{\partial}{\partial\theta} + \hat{e}_\phi \frac{1}{\sin\theta} \frac{\partial}{\partial\phi}\right] Y_{\ell m}(\theta, \phi)$$

$$\sqrt{\ell(\ell+1)}\ \underset{\sim}{C}_{\ell m} = \left[\hat{e}_\theta \frac{1}{\sin\theta} \frac{\partial}{\partial\phi} - \hat{e}_\phi \frac{\partial}{\partial\theta}\right] Y_{\ell m}(\theta, \phi) \qquad (2)$$

$$Y_{\ell m}(\theta, \phi) = P_{\ell m}(\cos\theta)\, e^{im\phi}$$

Then if we expand the Green's tensor and its derivatives, the displacement and the prestress in terms of these functions, the orthogonality relations:

$$\int \overline{P}_{\ell m} \cdot B_{\ell' m'} \, d\Omega = \int \overline{P}_{\ell m} \cdot C_{\ell' m'} \, d\Omega = \int \overline{B}_{\ell m} \cdot C_{\ell' m'} \, d\Omega = 0$$

and (3)

$$\int \overline{P}_{\ell m} \; P_{\ell' m'} \, d\Omega = \int \overline{B}_{\ell m} \cdot B_{\ell' m'} \, d\Omega = \int \overline{C}_{\ell m} \cdot C_{\ell' m'} \, d\Omega = \delta_{\ell \ell'} \delta_{m m'} \Omega_{\ell m}$$

$$\Omega_{\ell m} = \frac{4\pi}{2\ell + 1} \frac{(\ell + m)!}{(\ell - m)!}$$

used at the cavity surface ($\underset{\sim}{X} = \underset{\sim}{X}_0$) reduce equation (1) to a set of algebraic equations. Details of the solution may be found in Stevens (1980). Given the tractions in the form:

$$T(u^*) \cdot \hat{n} = \sum_{\ell=0}^{\infty} \sum_{m=-\ell}^{\ell} D_{\ell m}^{1} \; P_{\ell m}(\theta, \phi) + D_{\ell m}^{2} \sqrt{2(\ell + 1)} \; B_{\ell m}(\theta, \phi)$$

$$+ D_{\ell m}^{3} \sqrt{2(\ell + 1)} \; C_{\ell m}(\theta, \phi) \qquad (4)$$

the displacement may be expressed in terms of the elastic eigenvectors:

$$\underset{\sim}{u}(\underset{\sim}{x}, \omega) = \sum_{\ell=0}^{\infty} \sum_{m=-\ell}^{\ell} \alpha_{\ell m}(\omega) \, \underset{\sim}{M}_{\ell m}(\underset{\sim}{x}, \omega) + \beta_{\ell m}(\omega) \, \underset{\sim}{N}_{\ell m}(\underset{\sim}{x}, \omega)$$

$$+ \gamma_{\ell m}(\omega) \, \underset{\sim}{L}_{\ell m}(\underset{\sim}{x}, \omega) \qquad (5)$$

The coefficients $\alpha_{\ell m}$, $\beta_{\ell m}$, $\gamma_{\ell m}$ determine the displacement field at any point outside the cavity. The vector eigenfunctions

$\underset{\sim}{M}_{\ell m}$, $\underset{\sim}{N}_{\ell m}$, $\underset{\sim}{L}_{\ell m}$ represent toroidal, spheroidal shear, and spheroidal compressional waves respectively. They are defined by:

$$\underset{\sim}{M}_{\ell m} = f_\ell(y)\ \sqrt{\ell(\ell+1)}\ \underset{\sim}{C}_{\ell m}(\theta, \phi)$$

$$\underset{\sim}{N}_{\ell m} = \ell(\ell+1)\ \frac{f_\ell(y)}{y}\ \underset{\sim}{P}_{\ell m}(\theta, \phi)$$

$$+ \left(f'_\ell(y) + \frac{f_\ell(y)}{y}\right)\ \sqrt{\ell(\ell+1)}\ \underset{\sim}{B}_{\ell m}(\theta, \phi) \qquad (6)$$

$$\underset{\sim}{L}_{\ell m} = f'_\ell(x)\ \underset{\sim}{P}_{\ell m}(\theta, \phi) + \frac{f_\ell(x)}{x}\ \sqrt{\ell(\ell+1)}\ \underset{\sim}{B}_{\ell m}(\theta, \phi)$$

where $x = K_\alpha r$, $y = K_\beta r$, and $f_\ell = h_\ell^{(2)}$, the spherical Hankel function of the second kind.

APPENDIX 2

VECTOR MULTIPOLE COEFFICIENTS FOR PRESTRESS FIELDS

APPENDIX 2

VECTOR MULTIPOLE COEFFICENTS FOR PRESTRESS FIELDS

In order to use the preceeding solution it is necessary to have the initial stress field expanded in vector spherical harmonics:

$$T(\underset{\sim}{u^*}) \cdot \hat{n} = \sum_{\ell=0}^{\infty} \sum_{m=-\ell}^{\ell} D_{\ell m}^{1} \underset{\sim}{P}_{\ell m} + D_{\ell m}^{2} \sqrt{\ell(\ell+1)} \underset{\sim}{B}_{\ell m}$$

$$+ D_{\ell m}^{3} \sqrt{\ell(\ell+1)} \underset{\sim}{C}_{\ell m} \qquad (1)$$

The coefficients $D_{\ell m}^{1}$, $D_{\ell m}^{2}$, $D_{\ell m}^{3}$ may always be found by using the orthogonality relations of the vector harmonics, but in some cases they may be found analytically. A uniform stress field (σ_{ij} = constant) may be written in the form:

$$T(u^*) \cdot \hat{n} = A_{00} \underset{\sim}{P}_{00} + \sum_{m=-2}^{2} A_{2m} \left(\underset{\sim}{P}_{2m} + \frac{\sqrt{6}}{2} \underset{\sim}{B}_{2m}\right) \qquad (2)$$

with

$$A_{00} = \frac{1}{3} (\sigma_{11} + \sigma_{22} + \sigma_{33})$$

and defining the deviatoric stress tensor

$$\bar{\sigma}_{ij} = \sigma_{ij} - \delta_{ij} A_{00}$$

The remaining coefficients are:

$$A_{22} = \frac{1}{12} (\bar{\sigma}_{11} - \bar{\sigma}_{22}) + \frac{1}{6i} \sigma_{12}$$

$$A_{21} = \frac{1}{3} \sigma_{13} + \frac{i}{31} \sigma_{23} \tag{3}$$

$$A_{20} = \bar{\sigma}_{33}$$

The coefficients in equation (1) are then

$$D^1_{oo} = A_{oo}$$

$$D^1_{2m} = A_{2m} \tag{4}$$

$$D^2_{2m} = \frac{1}{2} A_{2m}$$

All other coefficients vanish.

The negative m values may always be determined from the positive m values by using the fact that the field is real. This requires that:

$$D^i_{\ell -m} = (-1)^m \frac{(\ell + m)!}{(\ell - m)!} \bar{D}^1_{\ell m} \tag{5}$$

($\bar{D}^i_{\ell m}$ is the complex conjugate of $D^i_{\ell m}$)

Two other prestress fields which may be expanded analytically are a point center of compression or a point dislocation located along the Z axis (see Figure A2-1).

The stress field for the center of compression may be easily found by using the fact that the (static) displacement field can be written

$$\underset{\sim}{u} = -\frac{c}{r^2} \hat{e}_r = c \nabla \frac{1}{r} \tag{6}$$

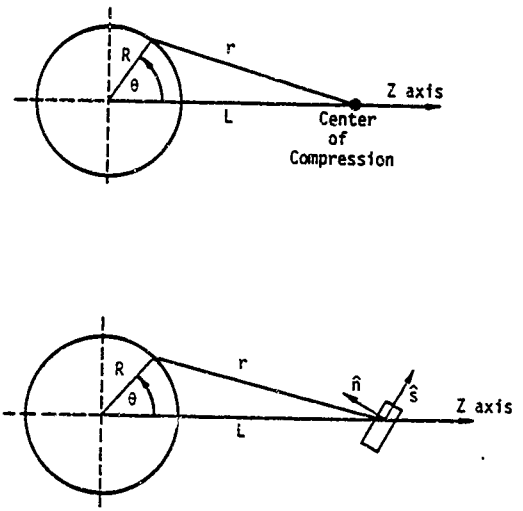

Figure A2.1. Coordinates used for computation of stress fields from center of compression and static dislocation.

Then expanding $\frac{1}{r}$ by:

$$\frac{1}{r} = \sum_{\ell=0}^{\infty} \frac{R^{\ell}}{L^{\ell+1}} P_{\ell}(\cos\theta) \qquad R<L \tag{7}$$

we find

$$\underset{\sim}{u} = \sum_{\ell=0}^{\infty} c \frac{R^{\ell}}{L^{\ell+1}} \underset{\sim}{P}_{\ell 0}(\cos\theta) \tag{8}$$

The tractions due to any displacement field of the form:

$$\underset{\sim}{u}(r, \theta, \phi) = \sum_{\ell,m} f_{1\ell m}(r) \underset{\sim}{P}_{\ell m} + f_{2\ell m}(r) \underset{\sim}{B}_{\ell m} + f_{3\ell m} \underset{\sim}{C}_{\ell m} \tag{9}$$

are given by

$$\begin{aligned} \underset{\sim}{\underset{\sim}{T}}(u)\cdot\hat{e}_r = \sum_{\ell m} & \left[\lambda \left(\frac{\partial f_{1\ell m}}{\partial r} + \frac{2 f_{1\ell m}}{r} - \sqrt{\ell(\ell+1)} \frac{f_{2\ell m}}{r} \right) \right. \\ & \left. + 2\mu \frac{\partial f_{1\ell m}}{\partial r} \right] \underset{\sim}{P}_{\ell m}(\theta, \phi) \\ & + \mu \left(\frac{\partial f_{2\ell m}}{\partial r} + \sqrt{\ell(\ell+1)} \frac{f_{1\ell m}}{r} - \frac{f_{2\ell m}}{r} \right) \underset{\sim}{B}_{\ell m}(\theta, \phi) \\ & + \mu \left(\frac{\partial f_{3\ell m}}{\partial r} - \frac{f_{3\ell m}}{r} \right) \underset{\sim}{C}_{\ell m}(\theta, \phi) \end{aligned} \tag{10}$$

So we find

$$\underset{\approx}{T}\,(\underset{\sim}{u^*}) \cdot \hat{e}_r = \frac{2\mu c}{L^3} \sum_{\ell=2}^{\infty} \left(\frac{R}{L}\right)^{\ell-2} \left[\ell(\ell-1)\ \underset{\sim}{P}_{\ell 0} + (\ell-1)\sqrt{\ell(\ell+1)}\ \underset{\sim}{B}_{\ell 0} \right] \tag{11}$$

so the coefficients become

$$D_{\ell 0}^{1} = \frac{2\mu c}{L^3} \left(\frac{R}{L}\right)^{\ell-2} \ell(\ell-1)$$

$$D_{\ell 0}^{2} = \frac{2\mu c}{L^3} \left(\frac{R}{L}\right)^{\ell-2} (\ell-1) \tag{12}$$

for $\ell \geq 2$. All other coefficients vanish.

The stress field for a point dislocation is more complicated. The displacement field due to the dislocation is given by the Volterra relation:

$$\underset{\sim}{u}\,(\underset{\sim}{x}) = \int \underset{\sim}{u}\,(\underset{\sim}{x_o}) \cdot \underset{\approx}{T}\,(\underset{\approx}{G}\,(\underset{\sim}{x}, \underset{\sim}{x_o})) \cdot \hat{n}\, dA_o \tag{13}$$

Here $\underset{\approx}{G}$ is the static elastic Green's tensor. For a point dislocation, this becomes:

$$\underset{\sim}{u^*}\,(\underset{\sim}{x}) = \underset{\sim}{S} \cdot \underset{\approx}{T}\,(\underset{\approx}{G}) \cdot \hat{n} \tag{14}$$

where $\underset{\sim}{S}$ is the slip vector $\underset{\sim}{S} = \Delta\underset{\sim}{u}A$ and $\hat{n}$ is the normal to the surface. We define the vector $\hat{S}$ to be a unit vector in the direction of slip. Then, using the analytic form for the Green's

tensor (Ben-Menahem and Singh, 1968) and applying the stress operator to equation (14), the stress field can be written:

$$\underset{\approx}{T}(\underset{\sim}{u}^*) \cdot \hat{e}_r \Big|_{r=R} = \frac{A\Delta u}{4\pi\mu} \sum_{\ell=0}^{\infty} \sum_{m=-\ell}^{\ell} \frac{(\ell-m)!}{(\ell+m)!}$$

$$\times \Big[\underset{\approx}{T}(\underset{\sim}{M}^+_{\ell m}) \cdot \hat{e}_r \left(\hat{n} \cdot \underset{\approx}{T}(\underset{\sim}{M}^{*-}_{\ell m}) \cdot \hat{\xi} \right) / \ell(\ell+1)$$

$$+ \underset{\approx}{T}(\underset{\sim}{N}^+_{\ell m}) \cdot \hat{e}_r \left(\hat{n} \cdot \underset{\approx}{T}(\underset{\sim}{F}^{*-}_{\ell m}) \cdot \hat{s} \right) / \ell(2\ell-1)$$

$$+ \underset{\approx}{T}(\underset{\sim}{F}^+_{\ell m}) \cdot \hat{e}_r \left(\hat{n} \cdot \underset{\approx}{T}(\underset{\sim}{N}^{*-}_{\ell m}) \cdot \hat{s} \right) / (\ell+1)(2\ell+3) \Big] \tag{15}$$

where the external eigenvectors are:

$$\underset{\sim}{N}^-_{\ell m} = r^{-\ell-2} \left[\sqrt{\ell(\ell+1)}\ \underset{\sim}{B}_{\ell m} - (\ell+1)\ \underset{\sim}{P}_{\ell m} \right]$$

$$\underset{\sim}{F}^-_{\ell m} = r^{-\ell} \frac{1}{\gamma} \left[(\gamma-\ell)\sqrt{\ell(\quad} \quad \underset{\sim}{B}_{\ell m} + (\gamma+\ell-1)\ell\, \underset{\sim}{P}_{\ell m} \right] \tag{16}$$

$$\underset{\sim}{M}^-_{\ell m} = r^{-\ell-1} \sqrt{\ell(\ell+1)}\ \underset{\sim}{C}_{\ell m}$$

where

$$\gamma = \frac{2\alpha^2}{\alpha^2 - \beta^2}$$

and the internal eigenvectors are:

$$\underset{\sim}{N}^+_{\ell m} = r^{\ell-1} \left[\sqrt{\ell(\ell+1)}\ \underset{\sim}{B}_{\ell m} + \underset{\sim}{P}_{\ell m} \right]$$

$$\underset{\sim}{F}^+_{\ell m} = r^{\ell+1} \frac{1}{\gamma} \left[(\ell+1+\gamma)\sqrt{\ell(\ell+1)}\ \underset{\sim}{B}_{\ell m} - (\gamma-\ell-2)(\ell+1)\ \underset{\sim}{P}_{\ell m} \right]$$

$$\underset{\sim}{M}^+_{\ell m} = r^{\ell} \sqrt{\ell(\ell+1)}\ \underset{\sim}{C}_{\ell m} \tag{17}$$

If the dislocation is located on the Z axis, then the calculation simplifies greatly as all terms with m > 2 vanish We need to evaluate the functions

$$\underset{\approx}{T}(\overset{*}{\underset{\sim}{H}}_{\ell m}),\ \underset{\approx}{T}(\overset{*}{\underset{\sim}{F}}_{\ell m}),\ \underset{\approx}{T}(\overset{*}{\underset{\sim}{N}}_{\ell m}) \text{ at } \theta = 0,\ \phi = 0,\ r = L$$

After some algebra and using simplifying relations from Ben-Menahem and Singh, 1968, p. 431), we find that the stresses associated with a vector of the form

$$\underset{\sim}{u} = f_1 \underset{\sim}{P}_{\ell m} + f_2 \sqrt{\ell(\ell+1)}\ \underset{\sim}{B}_{\ell m} + f_3 \sqrt{\ell(\ell+1)}\ \underset{\sim}{C}_{\ell m} \qquad (18)$$

can be written

$$\frac{1}{u}\underset{\approx}{T}(\underset{\sim}{u}) =$$

$$\begin{aligned}
&\hat{e}_r \hat{e}_r \left[2r \frac{d}{dr}\frac{f_1}{r} + \ell(\ell+1)\frac{f_2}{r} \right] \delta_{0m} \\
&\hat{e}_\theta \hat{e}_\theta \left[\frac{f_2}{r} + i\frac{f_3}{r} \right] \frac{1}{2}\frac{(\ell+2)!}{(\ell-2)!}\delta_{2m} \\
&\hat{e}_\phi \hat{e}_\phi \left[-\left(\frac{f_2}{r} + i\frac{f_3}{r} \right) \right] \frac{1}{2}\frac{(\ell+2)!}{(\ell-2)!}\delta_{2m} \\
&\hat{e}_r \hat{e}_\theta \left[\frac{f_1}{r} + r\frac{d}{dr}\frac{f_2}{r} + i\, r\frac{d}{dr}\frac{f_3}{r} \right] \frac{1}{2}\frac{(\ell+1)!}{(\ell-1)!}\delta_{1m} \\
&\hat{e}_r \hat{e}_\phi \left[i\frac{f_1}{r} + i\, r\frac{d}{dr}\frac{f_2}{r} - r\frac{d}{dr}\frac{f_3}{r} \right] \frac{1}{2}\frac{(\ell+1)!}{(\ell-1)!}\delta_{1m} \\
&\hat{e}_\theta \hat{e}_\phi \left[i\frac{f_2}{r} - \frac{f_3}{r} \right] \frac{1}{2}\frac{(\ell+2)!}{(\ell-2)!}\delta_{2m}
\end{aligned} \qquad (19)$$

For the static eigenvectors of interest, the functions f_1 are:

$$\underset{\sim}{F}_{\ell m}: \quad f_2 = r^{-\ell}\frac{\gamma-\ell}{\gamma} \qquad f_1 = r^{-\ell}\frac{\gamma+\ell-1}{\gamma}\,\ell$$

$$\underset{\sim}{N}_{\ell m}: \quad f_2 = r^{-(\ell+2)} \qquad f_1 = -(\ell+1)\,r^{-(\ell+2)} \tag{20}$$

$$\underset{\sim}{M}_{\ell m}: \quad f_3 = r^{-(\ell+1)}$$

We now define the coefficients A_M, A_F, A_N to be the complex conjugate of the right hand side of equation (19) double dotted with $\hat{n}$ and $\hat{s}$, evaluated using the functions f_1, f_2 and f_3 for the vectors $\underset{\sim}{M}_{\ell m}$, $\underset{\sim}{F}_{\ell m}$, and $\underset{\sim}{N}_{\ell m}$ respectively and divided by the Green's tensor factors $\ell(\ell+1)$, $\ell(2\ell-1)$, $(\ell+1)(2\ell+3)$ respectively. The tractions on the surface of the cavity are then:

$$\underset{\approx}{T}(\underset{\sim}{u})\cdot\hat{e}_r\Big|_{r=R} = \frac{A\Delta u}{4\pi}\sum_{\ell=0}^{\infty}\sum_{m=-2}^{2} A_M \underset{\approx}{T}(\underset{\sim}{M}^{+})\cdot\hat{e}_r + A_F \underset{\approx}{T}(\underset{\sim}{N}^{+})\cdot\hat{e}_r + A_N \underset{\approx}{T}(\underset{\sim}{F}^{+})\cdot\hat{e}_r \tag{21}$$

Finally, computing all quantities explicitly, we get:

$$\frac{4\pi}{A\Delta u}\quad D^1_{\ell m} = A_N\left[\lambda(\ell+1)(2-\gamma)(2\ell+3) + 2\mu(\ell+2-\gamma)(\ell+1)^2\right]\frac{R^\ell}{\gamma} + A_F\, 2\mu\,\ell(\ell-1)\,R^{\ell-2}$$

$$\frac{4\pi}{A\Delta\mu}\quad D^2_{\ell m} = A_N\,\mu\left(2(\ell+1)^2-\gamma\right)\frac{R^\ell}{\gamma} + A_F\,2\mu(\ell-1)\,R^{\ell-2} \tag{22}$$

$$\frac{4\pi}{A\Delta\mu}\quad D^3_{\ell m} = A_M\,\mu(\ell-1)\,R^{\ell-1}$$

APPENDIX 3

CONVERSION FROM VECTOR MULTIPOLE COEFFICIENTS TO SCALAR MULTIPOLE COEFFICIENTS

APPENDIX 3

CONVERSION FROM VECTOR MULTIPOLE COEFFICIENTS TO SCALAR MULTIPOLE COEFFICIENTS

In order to make synthetic seismograms in layered media, it is necessary to transform from vector spherical harmonics to vector cylindrical harmonics. The easiest way to do this is to first form the cartesian scalar potentials in spherical coordinates and then transform these to cylindrical coordinates.

The vector solutions are written:

$$\underset{\sim}{u}(\underset{\sim}{x}, \omega) = \sum_{\ell=0}^{\infty} \sum_{m=-\ell}^{\ell} \alpha_{\ell m}(\omega)\, \underset{\sim}{M}_{\ell m}(K_\beta r) + \beta_{\ell m}(\omega)\, \underset{\sim}{N}_{\ell m}(K_\beta r) + \gamma_{\ell m}(\omega)\, \underset{\sim}{L}_{\ell m}(K_\alpha r) \qquad (1)$$

The scalar potentials are written:

$$X^1 = \frac{1}{2}(\underset{\sim}{\nabla} \times \underset{\sim}{u})_i \qquad i = 1, 2, 3 \qquad (2)$$

$$X^4 = \underset{\sim}{\nabla} \cdot \underset{\sim}{u}$$

These are all harmonic functions and can be expanded in the form:

$$X^i = \sum_{\ell=0}^{\infty} \sum_{m=-\ell}^{\ell} A^i_{\ell m}\, \psi^i_{\ell m} \qquad (3)$$

where $\psi^i_{\ell m} = h^{(2)}_\ell (K_i r)\, P_{\ell m}(\cos\theta)\, e^{im\phi}$

Using the definitions:

$$\underset{\sim}{L}_{\ell m} = \frac{1}{K_\alpha} \nabla \psi^{\alpha}_{\ell m}$$

$$\underset{\sim}{M}_{\ell m} = \nabla \times r\hat{e}_r \psi^{\beta}_{\ell m} \tag{4}$$

$$\underset{\sim}{N}_{\ell m} = \frac{1}{K_\beta} \nabla \times \underset{\sim}{M}_{\ell m}$$

The problem is to determine the scalar coefficients $A^i_{\ell m}$ in terms of the vector coefficients $\alpha_{\ell m}$, $\beta_{\ell m}$, $\gamma_{\ell m}$. This is easily done for X^4.

$$X_4 = \nabla \cdot \underset{\sim}{u} = \sum_{\ell,m} \gamma_{\ell m} \quad \nabla \cdot \underset{\sim}{u} = \sum_{\ell,m} \gamma_{\ell m} \frac{1}{K_\alpha} \nabla^2 \psi^{\alpha}_{\ell m} = -k_\alpha \sum_{\ell,m} \gamma_{\ell m} \psi^{\alpha}_{\ell m}$$

Comparing with equation (3), the coefficient is:

$$A^4_{\ell m} = -k_\alpha \gamma_{\ell m} \tag{5}$$

Computation of X^i for i = 1, 3 is more difficult.

$$\frac{1}{2} \nabla \times \underset{\sim}{u} = \frac{1}{2} \sum_{\ell m} \alpha_{\ell m} \nabla \times \underset{\sim}{M}_{\ell m} + \beta_{\ell m} \nabla \times \underset{\sim}{N}_{\ell m} \tag{6}$$

$$= \frac{k_\beta}{2} \sum_{\ell m} \alpha_{\ell m} \underset{\sim}{N}_{\ell m} + \beta_{\ell m} \underset{\sim}{M}_{\ell m}$$

where the fact the $\nabla \cdot \underset{\sim}{M} = 0$ has been used. X^i then are the cartesian components of equation (6). Morse and Feshbach (1953) give the cartesian components of the vectors $\underset{\sim}{P}_{\ell m}$, $\underset{\sim}{B}_{\ell m}$ and $\underset{\sim}{C}_{\ell m}$ which can be used to reduce Equation 6 to scalar eigenfunctions:

$$\sqrt{2(\ell+1)}\ \underline{C}_{\ell m} = \frac{1}{2}\,\hat{i}\ \left[(\ell+m)(\ell-m+1)\,i\,Y_\ell^{m-1} + i\,Y_\ell^{m+1}\right]$$

$$-\frac{1}{2}\,\hat{j}\ \left[(\ell+m)(\ell-m+1)\,Y_\ell^{m-1} - Y_\ell^{m+1}\right] \qquad (7)$$

$$-\hat{k}\ im\ Y_\ell^m$$

Using $\underline{M}_{\ell m} = h_\ell^{(2)}\sqrt{\ell(\ell+1)}\ \underline{C}_{\ell m}$ and comparing with equation (3), we find:

$$\begin{aligned}
{}^{s}A^1_{\ell m} &= s_{\ell m+1}\frac{ik_s}{4}(\ell+m+1)(\ell-m) + s_{\ell m-1}\frac{ik_s}{4}\\
{}^{s}A^2_{\ell m} &= s_{\ell m+1}\frac{-k_s}{4}(\ell+m+1)(\ell-m) + s_{\ell m-1}\frac{k_s}{4} \qquad (8)\\
{}^{s}A^3_{\ell m} &= -\,im\,s_{\ell m}\frac{k_s}{2}
\end{aligned}$$

Similarly,

$$\underline{N}_{\ell m} = \frac{\ell(\ell+1)}{2\ell+1}\left(h_{\ell-1}^{(2)} + h_{\ell+1}^{(2)}\right)\underline{P}_{\ell m}$$

$$+\sqrt{\frac{\ell(\ell+1)}{2\ell+1}}\left((\ell+1)h_{\ell-1}^{(2)} - h_{\ell+1}^{(2)}\right)\underline{B}_{\ell m} \qquad (9)$$

where:

$$\underline{P}_{\ell m} = \frac{1}{2\ell+1}\left\{\frac{1}{2}\,\hat{i}\ \left[(\ell+m)(\ell+m-1)\,Y_{\ell-1}^{m-1} - Y_{\ell-1}^{m+1}\right.\right.$$

$$\left.-(\ell-m+1)(\ell-m+2)\,Y_{\ell+1}^{m-1} + Y_{\ell+1}^{m+1}\right]$$

$$+\frac{1}{2}\,\hat{j}\ \left[(\ell+m)(\ell+m-1)\,i\,Y_{\ell-1}^{m-1} + i\,Y_{\ell-1}^{m+1}\right.$$

$$\left.\left.-(\ell-m+1)(\ell-m+2)\,i\,Y_{\ell+1}^{m-1} - i\,Y_{\ell+1}^{m+1}\right]\right.$$

$$+ \hat{k} \left[(\ell + m)\, Y^m_{\ell-1} + (\ell - m + 1)\, Y^m_{\ell+1} \right] \Bigg\} \tag{10}$$

$$\sqrt{\ell(\ell+1)}\; \underline{B}_{\ell m} = \frac{1}{2\ell+1} \Bigg\{ \frac{1}{2}\hat{i} \Big[(\ell+1)(\ell+m)(\ell+m-1)\, Y^{m-1}_{\ell-1}$$

$$- (\ell+1)\, Y^{m+1}_{\ell-1}$$

$$+ \ell(\ell-m+1)(\ell-m+2)\, Y^{m-1}_{\ell+1} - \ell\, Y^{m+1}_{\ell+1} \Big]$$

$$+ \frac{1}{2}\hat{j} \Big[(\ell+1)(\ell+m)(\ell+m-1)\, i\, Y^{m-1}_{\ell-1}$$

$$+ (\ell+1)\, i\, Y^{m+1}_{\ell-1}$$

$$+ \ell(\ell-m+1)(\ell-m+2)\, i\, Y^{m-1}_{\ell+1}$$

$$+ \ell i\, Y^{m+1}_{\ell+1} \Big] \tag{11}$$

$$+ \hat{k} \left[(\ell+1)(\ell+m)\, Y^m_{\ell-1} - \ell(\ell-m+1)\, Y^m_{\ell+1} \right] \Bigg\}$$

All of the cross terms $\left(h^{(2)}_{\ell+1}\, Y^m_{\ell-1}, \text{ etc.} \right)$ cancel out as they must, leaving:

$$_{\alpha}A^1_{\ell m} = \frac{\kappa_g}{4} \Bigg[a_{\ell+1,\, m+1} \frac{(\ell+2)(\ell+m+2)(\ell+m+1)}{2\ell+3}$$

$$- a_{\ell+1,\, m-1} \frac{(\ell+2)}{2\ell+3}$$

$$- a_{\ell-1,\, m+1} \frac{(\ell-m-1)(\ell-m)(\ell-1)}{2\ell-1}$$

$$+ a_{\ell-1,\, m-1} \frac{(\ell-1)}{2\ell-1} \Bigg]$$

$$
{}_{\alpha}A^{2}_{\ell m} = \frac{ik_s}{4}\left[{}_{\alpha}a_{\ell+1,m+1}\ \frac{(\ell+2)(\ell+m+2)(\ell+m+1)}{2\ell+3} \right. \tag{12}
$$

$$
+ {}_{\alpha}a_{\ell+1,m-1}\ \frac{(\ell+2)}{2\ell+3}
$$

$$
+ {}_{\alpha}a_{\ell-1,m+1}\ \frac{(\ell-1-m)(\ell-m)(\ell-1)}{2\ell-1}
$$

$$
\left. + {}_{\alpha}a_{\ell-1,m-1}\ \frac{(\ell-1)}{2\ell-1} \right]
$$

$$
{}_{\alpha}A^{3}_{\ell m} = \frac{k_s}{2}\left[{}_{\alpha}a_{\ell+1,m}\ \frac{(\ell+2)(\ell+m+1)}{2\ell+3} + {}_{\alpha}a_{\ell-1,m}\ \frac{(\ell-1)(\ell-m)}{2\ell-1} \right]
$$

Equations (8) and (12) must be added for the complete multipole coefficients, that is:

$$
A^{i}_{\ell m} = {}_{\alpha}A^{i}_{\ell m} + {}_{\beta}A^{i}_{\ell m},\quad i = 1,\ 2,\ 3 \tag{13}
$$

This completes the transformations. However, it is sometimes convenient to have the coefficients expressed in the form:

$$
X = \sum_{\ell=0}^{\infty} \sum_{m=0}^{\ell} A^{R}_{\ell m}\, P_{\ell m}(\cos\theta)\, h^{(2)}_{\ell}(r)\cos m\phi
$$

$$
+ B^{R}_{\ell m}\, P_{\ell m}(\cos\theta)\, h^{(2)}_{\ell}(r)\sin m\phi \tag{14}
$$

Using the relation

$$
P^{-m}_{\ell}(\cos\theta) = (-1)^{m}\,\frac{(\ell-m)!}{(\ell+m)!}\,P^{m}_{\ell}(\cos\theta) \tag{15}
$$

We get

$$
A^{R}_{\ell 0} = A_{\ell 0}
$$

$$A^R_{\ell m} = A_{\ell m} + (-1)^m \frac{(\ell - m)!}{(\ell + m)!} A_{\ell -m} \qquad (16)$$

$$B^R_{\ell m} = 1 \left[A_{\ell m} - (-1)^m \frac{(\ell - m)!}{(\ell + m)!} A_{\ell -m} \right]$$

Minster (1976) gives the transformations for rotations of the multipole coefficients. The coefficients derived for stress concentrations along the z axis can be rotated to any other location.

The displacements may be recovered from the potentials using the relation:

$$\underset{\sim}{u}(\underset{\sim}{x}, \omega) = -\frac{1}{K_\alpha^2} \nabla \chi^4 + \frac{2}{K_\beta^2} \nabla \times \underset{\sim}{\chi}$$

Far field P waves have the simple form:

$$u^P = \frac{-e^{-iK_\alpha r}}{K_\alpha^2 r} \sum_\ell i^\ell \sum_m (A^4_{\ell m}(\omega) \cos m\phi + B^4_{\ell m}(\omega) \sin m\phi) P_{\ell m}(\cos\theta)$$

The scalar coefficients of equation (16) are now in the form used by Bache and Harkrider (1976) for computation of synthetic body wave seismograms and by Harkrider and Archambeau (1981) for computation of synthetic surface wave seismograms. These methods are used for all of the examples in this report.

APPENDIX 4

SCALING RELATIONS FOR MULTIPOLE COEFFICIENTS

APPENDIX 4

SCALING RELATIONS FOR MULTIPOLE COEFFICIENTS

The displacement field for tectonic release from a cavity of radius R can be written

$$u(\omega, r;R) = R^{\sim} \sum_{\ell,m} A_{\ell m}(R)\, f_{\ell}(\omega R)\, g_{\ell}(\omega r)$$

where $A_{\ell m}$ depends on the direction of observation and the type of prestress field, f_{ℓ} is a function of cavity radius and g_{ℓ} is a propagation term. If we change the cavity radius to R' leaving elastic constants the same, then

$$u(\omega, r; R') = (R')^2 \sum_{\ell,m} A_{\ell m}(R')\, f_{\ell}(\omega R')\, g_{\ell}(\omega r)$$

If we look at the displacement at frequency $\omega' = \frac{\omega R}{R'}$, then

$$u(\omega', r, R') = (R')^2 \sum_{\ell,m} A_{\ell m}(R')\, f_{\ell}(\omega R)\, g_{\ell}\left(\omega \frac{rR}{R'}\right)$$

For the case of constant prestress fields $A_{\ell m}(R') = A_{\ell m}(R)$ and we have the simple relation

$$u(\omega', r;R') = \left(\frac{R'}{R}\right)^2 u\left(\omega \frac{rR}{R'}, R\right)$$

In the far field g_{ℓ} is proportional to $1/\omega r$. Using

$$\frac{1}{\omega' r} = \frac{R'}{\omega r R}$$

we get

$$u(\omega', r;R') = \left(\frac{R'}{R}\right)^3 u(\omega, r; R)$$

so the displacement varies as the cube of the radius at a frequency which varies inversely with radius.

Similarly, for the inhomogeneous stress fields considered, the coefficients have the form

$$A_{2m}(R') = \frac{1}{L^3} F_{2m}\left(\frac{R}{L}\right)$$

If we vary the stress field so that $\frac{R}{L}$ = constant, then

$$u(\omega', r;R') = \left(\frac{R'}{R}\right)^3 \left(\frac{L}{L'}\right)^3 u(\omega, r; R) = u(\omega, r; R)$$

If, however, we use the maximum stress (or average stress) as a parameter, the scaling for homogeneous and inhomgeneous stress fields becomes the same.

For homogeneous stress fields the displacement is proportional to the prestress. For the stress concentrations, the stress field is proportional to $1/L^3$. If R/L is constant, then the stress field at all points on the surface scales as L^{-3}. So, using the stress (at any point) σ as a parameter, the scaling relation for all of the stress fields becomes

$$u\left(\frac{R}{R'}\omega, r;R'\right) = \frac{\sigma'(R')^3}{\sigma R^3} u(\omega, r;R)$$

At low frequencies the spectrum is approximately flat so the displacement (and the generation of surface waves) are proportional to σR^3. At high frequencies the spectrum is proportional to ω^{-2} so the displacements scale with σR.